

CERN-PH-TH/2004-232

MC-TH-2004-04

hep-ph/0411379

November 2004

# Resonant CP Violation in MSSM Higgs Production and Decay at $\gamma\gamma$ Colliders

John Ellis<sup>a</sup>, Jae Sik Lee<sup>b</sup> and Apostolos Pilaftsis<sup>b</sup>

<sup>a</sup>*Theory Division, Physics Department, CERN, CH-1211 Geneva 23, Switzerland*

<sup>b</sup>*School of Physics and Astronomy, University of Manchester  
Manchester M13 9PL, United Kingdom*

## ABSTRACT

We study CP-violating phenomena in the production, mixing and decay of a coupled system of CP-violating neutral Higgs bosons at  $\gamma\gamma$  colliders, assuming a Minimal Supersymmetric Standard Model (MSSM) Higgs sector in which CP violation is radiatively induced by phases in the soft supersymmetry-breaking gaugino masses and third-generation trilinear squark couplings. We discuss CP asymmetries in the production and decays of  $\mu^+\mu^-$ ,  $\tau^+\tau^-$ ,  $\bar{b}b$  and  $\bar{t}t$  pairs. We find large asymmetries when two (or all three) neutral Higgs bosons are nearly degenerate with mass differences comparable to their decay widths, as happens naturally in the CP-violating MSSM for values of  $\tan\beta \gtrsim 5$  (30) and large (small) charged Higgs-boson masses.

# 1 Introduction

The Minimal Supersymmetric extension of the Standard Model (MSSM) [1] offers many possible sources of CP violation beyond the single Kobayashi–Maskawa phase in the Standard Model (SM). However, if the soft supersymmetry-breaking parameters  $m_0, m_{1/2}$  and  $A$  are universal, only two new physical CP-odd phases remain: one in the trilinear couplings  $A$  and one in the gaugino masses  $m_{1/2}$ . If Nature is described by such a constrained CP-violating version of the MSSM, the production and decays of sparticles would offer many direct signatures of these new CP-violating parameters at high-energy colliders [2–4]. Additional indirect signatures could be provided by their radiative effects on the Higgs sector [5], electric dipole moments (EDMs) [6–8] and  $B$ -meson observables [9, 10].

The Higgs sector of the MSSM is affected, to a greater extent, by the trilinear phase at the one-loop level [5, 11–19], and, to a lesser extent, by the gaugino mass phases at the one- and two-loop levels [13–16]. A complete treatment of this loop-induced CP violation involves a careful consideration of the three-way mixing between the CP-even Higgses  $h, H$  and the CP-odd Higgs boson  $A$ , including off-diagonal absorptive effects in the resummed Higgs-boson propagator matrix [20, 21]. Many studies have been made of the masses, couplings, production and decays of the resulting mixed-CP Higgs bosons  $H_{1,2,3}$ , with a view to searches at LEP [22] and future colliders, such as the LHC [22–27], the International  $e^+e^-$  Linear Collider (ILC) [28], a  $\mu^+\mu^-$  collider [29] and a  $\gamma\gamma$  collider [30–33]. The main purpose of this paper is to extend the treatment of three-way mixing given previously in [21] to  $\gamma\gamma$  colliders.

The  $\gamma\gamma$  colliders offer unique capabilities for probing CP violation in the MSSM Higgs sector, because one may vary the initial-state polarizations as well as measure the polarizations of some final states in Higgs decays. We illustrate these capabilities by considering coupled-channel  $H_{1,2,3}$  mixing in  $\mu^+\mu^-$ ,  $\tau^+\tau^-$ ,  $\bar{b}b$  and  $\bar{t}t$  final states. Even with quite small CP-violating phases, sizable CP-violating effects are possible when  $\tan\beta$  is large and/or the charged Higgs boson mass is large, so that two or three Higgs bosons are nearly degenerate, as we demonstrate in a couple of specific scenarios. One of these exhibits large mixing between three near-degenerate MSSM Higgs bosons  $H_{1,2,3}$ , and the other scenario features one lighter Higgs boson  $H_1$  and two heavier states  $H_{2,3}$ .

The layout of this paper is as follows. Section 2 provides basic formulae for the  $\gamma\gamma \rightarrow \bar{f}f$  cross sections, including the QED continuum background as well as the Higgs contribution, and introducing CP-conserving and CP-violating observables in polarized  $\gamma\gamma$  collisions. In this connection, we also review the formalism for three-way Higgs mixing, stressing the key role played by off-diagonal absorptive parts. Section 3 presents model

calculations of cross sections and CP-violating asymmetries in  $\tau^+\tau^-$  and  $\bar{b}b$  final states in a specific scenario with strong three-way neutral-Higgs mixing. Section 4 discusses  $\bar{t}t$  final states in a scenario with two strongly-mixed heavy neutral Higgs bosons. Finally, Section 5 summarizes our conclusions and presents some prospects for future work.

## 2 Polarization-Dependent Cross Sections in $\gamma\gamma$ Collisions

We study in this Section the processes  $\gamma\gamma \rightarrow f\bar{f}$ , where  $f = \mu^-, \tau^-, b$ , or  $t$ . We consider three separate cases for the helicities of the initial-state photons and the final-state fermions, and present a classification of all the polarization-dependent cross sections according to their CP and CPT $\tilde{T}$  parities.

### 2.1 QED Continuum Background

The tree-level Feynman diagrams for the QED process  $\gamma\gamma \rightarrow \bar{f}f$  are shown in Fig. 1. In the two-photon centre-of-mass (c.o.m.) system, the helicity amplitudes for the QED production of a fermion-antifermion pair take the forms:

$$\mathcal{M}_C = 4\pi\alpha Q_f^2 \langle \sigma \bar{\sigma}; \lambda_1 \lambda_2 \rangle_C, \quad (2.1)$$

where

$$\begin{aligned} \langle \sigma \sigma; \lambda \lambda \rangle_C &= \frac{4m_f}{\sqrt{\hat{s}}} \frac{1}{1 - \beta_f^2 c_\theta^2} (\lambda + \sigma\beta_f), \\ \langle \sigma \sigma; \lambda - \lambda \rangle_C &= -\frac{4m_f}{\sqrt{\hat{s}}} \frac{s_\theta^2}{1 - \beta_f^2 c_\theta^2} \sigma\beta_f, \\ \langle \sigma - \sigma; \lambda \lambda \rangle_C &= 0, \\ \langle \sigma - \sigma; \lambda - \lambda \rangle_C &= -2\beta_f \frac{s_\theta}{1 - \beta_f^2 c_\theta^2} (\sigma\lambda + c_\theta), \end{aligned} \quad (2.2)$$

where  $s_\theta \equiv \sin\theta$  and  $c_\theta \equiv \cos\theta$  with  $\theta$  the angle between  $\mathbf{p}_1$  and  $\mathbf{k}_1$ , and  $\beta_f \equiv \sqrt{1 - 4m_f^2/\hat{s}}$  with  $\hat{s} = (k_1 + k_2)^2 = (p_1 + p_2)^2$ . We allow for independent and measurable polarizations  $\lambda_{1,2}$  of the initial-state photons and  $\bar{\sigma}, \sigma$  of the final-state fermion-antifermion pair. We note that the last amplitude in (2.2) with completely different helicity states is the least important, since the Higgs-mediated diagram is non-vanishing only when the helicities of photons and/or those of final fermions are equal.

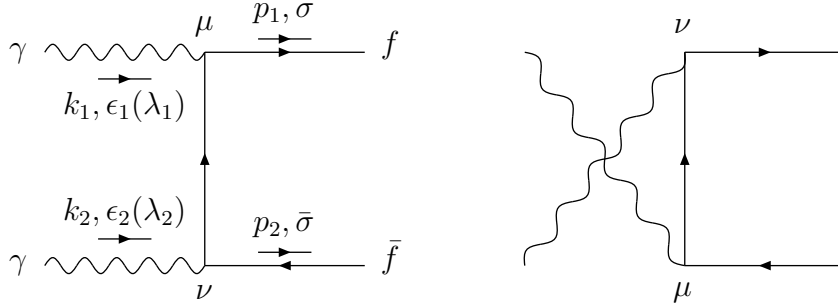


**Figure 1:** Feynman diagrams contributing to the tree-level QED background, introducing our definitions of the initial-state photon and final-state fermion momenta and helicities.

## 2.2 Coupled-Channel Analysis of Processes Mediated by Higgs Bosons

We now discuss how mixed Higgs bosons may contribute to the various  $\gamma\gamma \rightarrow \bar{f}f$  helicity amplitudes, interfering with the above QED amplitudes and, in some cases, violating either CP and/or invariance under the  $C\tilde{P}\tilde{T}$  transformation defined below.

In situations where two or more MSSM Higgs bosons contribute simultaneously to the production of some fermion-antifermion pair, one should consider [21]\* the ‘full’  $3 \times 3$  Higgs-boson propagator matrix  $D(\hat{s})$ , including off-diagonal absorptive parts <sup>†</sup>. This is given by

$$D(\hat{s}) = \hat{s} \begin{pmatrix} \hat{s} - M_{H_1}^2 + i\Im\hat{\Pi}_{11}(\hat{s}) & i\Im\hat{\Pi}_{12}(\hat{s}) & i\Im\hat{\Pi}_{13}(\hat{s}) \\ i\Im\hat{\Pi}_{21}(\hat{s}) & \hat{s} - M_{H_2}^2 + i\Im\hat{\Pi}_{22}(\hat{s}) & i\Im\hat{\Pi}_{23}(\hat{s}) \\ i\Im\hat{\Pi}_{31}(\hat{s}) & i\Im\hat{\Pi}_{32}(\hat{s}) & \hat{s} - M_{H_3}^2 + i\Im\hat{\Pi}_{33}(\hat{s}) \end{pmatrix}^{-1}, \quad (2.3)$$

where  $M_{H_{1,2,3}}$  are the one-loop Higgs-boson pole masses, and higher-order absorptive effects on  $M_{H_{1,2,3}}$  have been ignored [16]. The absorptive part of the Higgs-boson propagator matrix receives contributions from loops of fermions, vector bosons, associated pairs of Higgs and vector bosons, Higgs-boson pairs, and sfermions:

$$\Im\hat{\Pi}_{ij}(s) = \Im\hat{\Pi}_{ij}^{ff}(s) + \Im\hat{\Pi}_{ij}^{VV}(s) + \Im\hat{\Pi}_{ij}^{HV}(s) + \Im\hat{\Pi}_{ij}^{HH}(s) + \Im\hat{\Pi}_{ij}^{\tilde{f}\tilde{f}}(s), \quad (2.4)$$

\*For an alternative approach, see Ref. [33].

<sup>†</sup>As commented in [21], the complete propagator matrix  $D(\hat{s})$  is a  $4 \times 4$ -dimensional matrix spanned by the basis  $(H_1, H_2, H_3, G^0)$  [20]. However, the small off-resonant self-energy transitions of the Higgs bosons  $H_{1,2,3}$  to the neutral would-be Goldstone boson  $G^0$  may safely be neglected for our purposes.

respectively. We use the pinch technique (PT) [34] to evaluate the contributions from pairs of vector bosons and associated pairs of Higgs and vector bosons, following the procedure used in [35] for the SM Higgs sector.

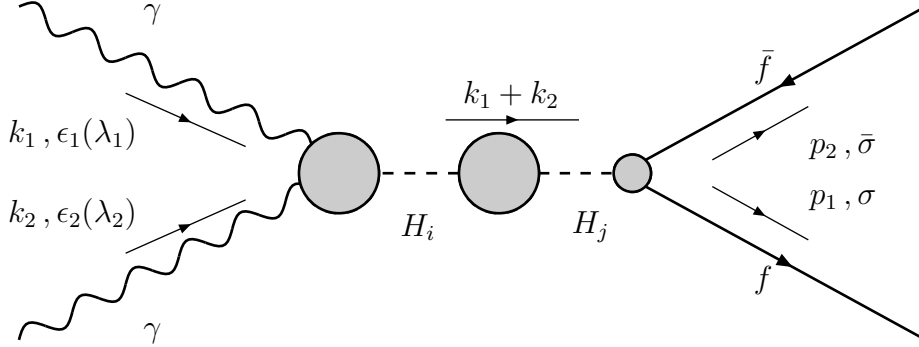


**Figure 2:** Mechanisms contributing to the process  $\gamma\gamma \rightarrow H_{1,2,3} \rightarrow \bar{f}f$ , including off-diagonal absorptive parts in the Higgs-boson propagator matrix.

The helicity amplitudes contributing to  $\gamma\gamma \rightarrow H \rightarrow \bar{f}f$ , see Fig. 2, are given by

$$\mathcal{M}_H = \frac{\alpha m_f \sqrt{\hat{s}}}{4\pi v^2} \langle \sigma; \lambda_1 \rangle_H \delta_{\sigma\bar{\sigma}} \delta_{\lambda_1 \lambda_2}, \quad (2.5)$$

where the reduced amplitude

$$\langle \sigma; \lambda \rangle_H = \sum_{i,j=1}^3 [S_i^\gamma(\sqrt{\hat{s}}) + i\lambda P_i^\gamma(\sqrt{\hat{s}})] D_{ij}(\hat{s}) (\sigma \beta_f g_{H_j \bar{f}f}^S - i g_{H_j \bar{f}f}^P), \quad (2.6)$$

is a quantity given by the Higgs-boson propagator matrix (2.3) combined with the production and decay vertices. The one-loop induced complex couplings of the  $\gamma\gamma H_i$  vertex,  $S_i^\gamma(\sqrt{\hat{s}})$  and  $P_i^\gamma(\sqrt{\hat{s}})$ , get dominant contributions from charged particles such as the bottom and top quarks, tau leptons,  $W^\pm$  bosons, charginos, third-generation sfermions and charged Higgs bosons. Relevant aspects of the loop-induced corrections to the  $H_j f \bar{f}$  vertices were discussed in [21]. We follow the convention of CPsuperH [36] for the couplings of the Higgs bosons.

For future reference, we note the following properties of the  $\gamma\gamma \rightarrow \bar{f}f$  helicity amplitudes under the CP transformation:

$$\langle \sigma \bar{\sigma}; \lambda_1 \lambda_2 \rangle \xleftrightarrow{\text{CP}} (-1)(-1)^{(\sigma-\bar{\sigma})/2} \langle -\bar{\sigma} - \sigma; -\lambda_2 - \lambda_1 \rangle. \quad (2.7)$$

Also interesting are the properties under the CPT $\tilde{T}$  transformation, where  $\tilde{T}$  reverses the signs of the spins and the three-momenta of the asymptotic states, without interchanging

initial and final states, and the matrix element gets complex conjugated:

$$\langle \sigma \bar{\sigma}; \lambda_1 \lambda_2 \rangle \xrightarrow{\text{CPT}} (-1)(-1)^{(\sigma-\bar{\sigma})/2} \langle -\bar{\sigma} - \sigma; -\lambda_2 - \lambda_1 \rangle^*. \quad (2.8)$$

Evidently, the QED helicity amplitudes (2.2) are even under both the CP and CPT transformations. On the other hand, the simultaneous presence of  $\{S_i^\gamma, P_i^\gamma\}$  and/or  $\{g_{H_j \bar{f} f}^S, g_{H_j \bar{f} f}^P\}$  would signal CP violation in the Higgs-boson-exchange amplitude (2.6), and non-vanishing absorptive parts from the vertices and the propagators could also lead to CPT violation in the Higgs-exchange diagram.

It is convenient to distinguish three distinct cases for the helicities of the initial-state photons and final-state fermions.

### 2.3 Case I: Identical photon and fermion helicities

The first case is that of identical photon and fermion helicities, in which case the amplitude may be written as

$$\mathcal{M}_{\sigma\lambda}^I = \mathcal{M}_C|_{\bar{\sigma}=\sigma, \lambda_1=\lambda_2=\lambda} + \mathcal{M}_H = \frac{\alpha m_f \sqrt{\hat{s}}}{4\pi v^2} \langle \sigma; \lambda \rangle \quad (2.9)$$

where  $\mathcal{M}_C$  was given in (2.1),  $\mathcal{M}_H$  was given in (2.5) and we have

$$\langle \sigma; \lambda \rangle \equiv \langle \sigma; \lambda \rangle_H + R(\hat{s})f(\theta)\langle \sigma; \lambda \rangle_C. \quad (2.10)$$

The previous discussion of the QED amplitude  $\mathcal{M}_C$  (2.1) yields

$$\begin{aligned} R(\hat{s}) &= 64\pi^2 Q_f^2 v^2 / \hat{s}, \\ f(\theta) &= 1/(1 - \beta_f^2 c_\theta^2), \\ \langle \sigma; \lambda \rangle_C &= \lambda + \sigma \beta_f, \end{aligned} \quad (2.11)$$

and we note that  $\langle \pm; \mp \rangle_C = \mp(1 - \beta_f)$ , which vanishes in the limit  $m_f \rightarrow 0$ .

Corresponding to the different combinations of helicities of the initial-state photons and final-state fermions, we have four cross sections:

$$\frac{d\hat{\sigma}_{\sigma\lambda}}{dc_\theta} = \frac{\beta_f N_C}{32\pi \hat{s}} \left| \mathcal{M}_{\sigma\lambda}^I \right|^2 \quad (2.12)$$

where  $\sigma, \lambda = \pm$ . After integrating over  $c_\theta$ , we have

$$\hat{\sigma}_{\sigma\lambda} = \frac{\beta_f N_C}{32\pi} \left( \frac{\alpha m_f}{4\pi v^2} \right)^2 \mathcal{Y}_{\sigma\lambda} \quad (2.13)$$

with

$$\begin{aligned} \mathcal{Y}_{\sigma\lambda} \equiv \int_{-z_f}^{z_f} dc_\theta |\langle\sigma; \lambda\rangle|^2 &= 2 |\langle\sigma; \lambda\rangle_H|^2 + 2R(\hat{s})^2 F_1^{z_f} |\langle\sigma; \lambda\rangle_C|^2 \\ &+ 2R(\hat{s}) F_2^{z_f} \Re(\langle\sigma; \lambda\rangle_H \langle\sigma; \lambda\rangle_C^*). \end{aligned} \quad (2.14)$$

The functions  $F_1^{z_f}$  and  $F_2^{z_f}$  are given by

$$\begin{aligned} F_1^{z_f} &= \frac{1}{2} \int_{-z_f}^{z_f} dc_\theta f^2(\theta) = \frac{z_f}{2(1 - z_f^2 \beta_f^2)} + \frac{\ln \frac{1+z_f \beta_f}{1-z_f \beta_f}}{4\beta_f}, \\ F_2^{z_f} &= \int_{-z_f}^{z_f} dc_\theta f(\theta) = \frac{\ln \frac{1+z_f \beta_f}{1-z_f \beta_f}}{\beta_f}. \end{aligned} \quad (2.15)$$

Note that we have introduced an experimental cut on the fermion polar angle  $\theta$ :  $|\cos\theta| \leq z_f$  and  $\cos\theta_{\text{cut}}^f = z_f$ . Experimentally, we can not measure the final state fermion if it has too small angle  $\theta$  outside the coverage of detectors. This angular cut has significant effects in the cases of light fermions,  $f = \mu, \tau$ , and  $b$ , since the QED continuum cross section  $\hat{\sigma}_C$ , or  $F_1^{z_f}$ , strongly depends on it. Actually we find that the QED cross sections are suppressed by factors of about 5000 and 20 for  $f = \mu$  and  $f = \tau$  cases, respectively, by imposing  $\theta_{\text{cut}}^{\mu, \tau} = 130$  mrad angle cut ( $z_{\mu, \tau} \simeq 0.99$ ) when  $\sqrt{\hat{s}} = 120$  GeV. For  $b$ -quark case, the suppression factor is about 30 imposing  $\theta_{\text{cut}}^b = 280$  mrad ( $z_b \simeq 0.96$ ). On the other hand, the Higgs-mediated cross section and the QED continuum cross section for top quarks are hardly affected by the polar angle cut. The introduction on the polar angle cut, therefore, greatly enhance the significance of the Higgs-mediated process with respect to the QED continuum one for  $f = \mu, \tau$ , and  $b$ .

The helicity-averaged cross section is

$$\hat{\sigma} = \frac{1}{4} (\hat{\sigma}_{++} + \hat{\sigma}_{--} + \hat{\sigma}_{+-} + \hat{\sigma}_{-+}). \quad (2.16)$$

We can construct two CP-violating cross sections in terms of  $\hat{\sigma}_{\sigma\lambda}$ :

$$\hat{\Delta}_1 \equiv \hat{\sigma}_{++} - \hat{\sigma}_{--}, \quad \hat{\Delta}_2 \equiv \hat{\sigma}_{+-} - \hat{\sigma}_{-+}, \quad (2.17)$$

or, equivalently, the two linear combinations

$$(\hat{\Delta}_1 + \hat{\Delta}_2) = \sum_{\lambda=\pm} (\hat{\sigma}_{+\lambda} - \hat{\sigma}_{-\lambda}), \quad (\hat{\Delta}_1 - \hat{\Delta}_2) = \sum_{\sigma=\pm} (\hat{\sigma}_{\sigma+} - \hat{\sigma}_{\sigma-}). \quad (2.18)$$

The CP-violating cross section  $(\hat{\Delta}_1 - \hat{\Delta}_2)$  can be measured without determining the helicities of the final-state fermions.

Finally, the QED continuum contribution is given by

$$\hat{\sigma}_C = \frac{\beta_f N_C}{16\pi} \left( \frac{\alpha m_f}{4\pi v^2} \right)^2 \frac{R(\hat{s})^2 F_1^{z_f} \sum_{\sigma, \lambda = \pm} |\langle \sigma; \lambda \rangle_C|^2}{4}. \quad (2.19)$$

Note that, when  $z_{\mu, \tau, b} = 1$ , the leading term of  $\hat{\sigma}_C$  is proportional to  $N_C Q_f^4$  with a factor  $m_f^2$  cancelled. But with  $z_f \lesssim 0.99$ ,  $F_1^{z_f}$  becomes nearly independent of fermion species and the cross section is proportional to  $N_C m_f^2 Q_f^4$ .

## 2.4 Case II: Identical fermion helicities

In this case, there are two possible final-state fermion helicity states to consider, so the amplitude becomes a matrix:

$$\left( \mathcal{M}_\sigma^{\text{II}} \right)_{\lambda_1 \lambda_2} = \frac{\alpha m_f \sqrt{\hat{s}}}{4\pi v^2} \begin{pmatrix} \langle \sigma; + \rangle & \langle \sigma \rangle_C \\ \langle \sigma \rangle_C & \langle \sigma; - \rangle \end{pmatrix} \quad (2.20)$$

where  $\sigma = \pm$ ,

$$\langle \sigma \rangle_C \equiv -R(\hat{s}) s_\theta^2 f(\theta) \sigma \beta_f, \quad (2.21)$$

and the  $\langle \sigma; \lambda \rangle$  were defined in (2.10).

The polarization density matrices for the two photons are:

$$\tilde{\rho} = \frac{1}{2} \begin{pmatrix} 1 + \tilde{\zeta}_2 & -\tilde{\zeta}_3 + i\tilde{\zeta}_1 \\ -\tilde{\zeta}_3 - i\tilde{\zeta}_1 & 1 - \tilde{\zeta}_2 \end{pmatrix}, \quad \rho = \frac{1}{2} \begin{pmatrix} 1 + \zeta_2 & -\zeta_3 + i\zeta_1 \\ -\zeta_3 - i\zeta_1 & 1 - \zeta_2 \end{pmatrix}, \quad (2.22)$$

where the  $\zeta_i$  ( $\tilde{\zeta}_i$ ) are the Stokes parameters which describe the polarization transfer from the initial laser light and electron (positron) to the colliding photon:  $\zeta_2$  is the degree of circular polarization and  $(\zeta_3, \zeta_1)$  are the degrees of linear polarization transverse and normal to the plane defined by the electron direction and the direction of the maximal linear polarization of the initial laser light. The polarization-weighted squared matrix elements can be obtained by [37]

$$|\mathcal{M}_\sigma^{\text{II}}|^2 = \text{Tr} \left[ \mathcal{M}_\sigma^{\text{II}} \tilde{\rho} \mathcal{M}_\sigma^{\text{II}\dagger} \rho^T \right]. \quad (2.23)$$

The initial-spin average factor has already been included in the spin density matrices, so that summing over  $\zeta_i, \tilde{\zeta}_i$  and  $\sigma$  gives the total cross section. The amplitude squared can therefore be written as

$$\begin{aligned} |\mathcal{M}_\sigma^{\text{II}}|^2 &= \left( \frac{\alpha m_f \sqrt{\hat{s}}}{4\pi v^2} \right)^2 \\ &\times \left\{ A_1^\sigma (1 + \zeta_2 \tilde{\zeta}_2) + A_2^\sigma [(\zeta_1 \tilde{\zeta}_1 - \zeta_2 \tilde{\zeta}_2) + (\zeta_3 \tilde{\zeta}_3 - \zeta_2 \tilde{\zeta}_2)] \right\} \end{aligned}$$



$$\begin{aligned}
& +B_1^\sigma(\zeta_2 + \tilde{\zeta}_2) + B_2^\sigma(\zeta_1\tilde{\zeta}_3 + \zeta_3\tilde{\zeta}_1) + B_3^\sigma(\zeta_3\tilde{\zeta}_3 - \zeta_1\tilde{\zeta}_1) \\
& +C_1^\sigma(\zeta_1 + \tilde{\zeta}_1) + C_2^\sigma(\zeta_3 + \tilde{\zeta}_3) + C_3^\sigma(\zeta_1\tilde{\zeta}_2 + \zeta_2\tilde{\zeta}_1) + C_4^\sigma(\zeta_2\tilde{\zeta}_3 + \zeta_3\tilde{\zeta}_2) \Big\},
\end{aligned}$$

where

$$\begin{aligned}
A_1^\sigma &= \frac{1}{4} \left( |\langle\sigma; +\rangle|^2 + |\langle\sigma; -\rangle|^2 + 2|\langle\sigma\rangle_C|^2 \right), \\
A_2^\sigma &= \frac{1}{2} |\langle\sigma\rangle_C|^2, \\
B_1^\sigma &= \frac{1}{4} \left( |\langle\sigma; +\rangle|^2 - |\langle\sigma; -\rangle|^2 \right), \\
B_2^\sigma &= \frac{1}{2} \Im[\langle\sigma; +\rangle \langle\sigma; -\rangle^*], \\
B_3^\sigma &= \frac{1}{2} \Re[\langle\sigma; +\rangle \langle\sigma; -\rangle^*], \\
C_1^\sigma &= -\frac{1}{2} \Im[(\langle\sigma; +\rangle - \langle\sigma; -\rangle) \langle\sigma\rangle_C^*], \\
C_2^\sigma &= -\frac{1}{2} \Re[(\langle\sigma; +\rangle + \langle\sigma; -\rangle) \langle\sigma\rangle_C^*], \\
C_3^\sigma &= -\frac{1}{2} \Im[(\langle\sigma; +\rangle + \langle\sigma; -\rangle) \langle\sigma\rangle_C^*], \\
C_4^\sigma &= -\frac{1}{2} \Re[(\langle\sigma; +\rangle - \langle\sigma; -\rangle) \langle\sigma\rangle_C^*]. \tag{2.24}
\end{aligned}$$

We note that the quantities  $B_{2,3}^\sigma$  are related to the observables in the interference between the amplitudes with different photon helicities requiring linear polarizations of the colliding photon beams, and that the observables  $C_i^\sigma$  are due to interference with the QED continuum.

We distinguish two categories of cross sections, according to the final-state fermion helicity  $\sigma$ :

$$\begin{aligned}
\frac{d\hat{\Sigma}^X}{dc_\theta} &\equiv \frac{\beta_f N_C}{32\pi} \left( \frac{\alpha m_f}{4\pi v^2} \right)^2 (X^+ + X^-), \\
\frac{d\hat{\Delta}^X}{dc_\theta} &\equiv \frac{\beta_f N_C}{32\pi} \left( \frac{\alpha m_f}{4\pi v^2} \right)^2 (X^+ - X^-), \tag{2.25}
\end{aligned}$$

where  $X = A_i, B_j, C_k$ . We define the following quantities obtained by integration over the angle  $\theta$ :

$$\begin{aligned}
\mathcal{W}_\sigma &\equiv \int_{-z_f}^{z_f} dc_\theta |\langle\sigma\rangle_C|^2 = \beta_f^2 R(\hat{s})^2 F_3^{z_f}, \\
\mathcal{X}_\sigma &\equiv \int_{-z_f}^{z_f} dc_\theta \langle\sigma; +\rangle \langle\sigma; -\rangle^* = 2\langle\sigma; +\rangle_H \langle\sigma; -\rangle_H^* + 2R(\hat{s})^2 F_1^{z_f} \langle\sigma; +\rangle_C \langle\sigma; -\rangle_C^* \\
&\quad + R(\hat{s}) F_2^{z_f} (\langle\sigma; +\rangle_C \langle\sigma; -\rangle_H^* + \langle\sigma; +\rangle_H \langle\sigma; -\rangle_C^*), \\
\mathcal{Z}_{\sigma\lambda} &\equiv \int_{-z_f}^{z_f} dc_\theta \langle\sigma; \lambda\rangle \langle\sigma\rangle_C^* = -\sigma\beta_f R(\hat{s}) \left[ F_4^{z_f} \langle\sigma; \lambda\rangle_H + R(\hat{s}) F_5^{z_f} \langle\sigma; \lambda\rangle_C \right], \tag{2.26}
\end{aligned}$$

and define  $\mathcal{Y}_{\sigma\lambda}$  as in (2.14). In addition to the functions  $F_{1,2}^{z_f}$  given in (2.15), the functions  $F_{3,4,5}^{z_f}$  are

$$\begin{aligned} F_3^{z_f} &= \int_{-z_f}^{z_f} dc_\theta s_\theta^4 f^2(\theta) = \frac{[3 - 2(1 + z_f^2)\beta_f^2 + \beta_f^4] z_f}{\beta_f^4 (1 - z_f^2 \beta_f^2)} - \frac{\ln \frac{1+z_f\beta_f}{1-z_f\beta_f}}{2\beta_f^5} (1 - \beta_f^2)(3 + \beta_f^2), \\ F_4^{z_f} &= \int_{-z_f}^{z_f} dc_\theta s_\theta^2 f(\theta) = \frac{2 z_f}{\beta_f^2} - \frac{\ln \frac{1+z_f\beta_f}{1-z_f\beta_f}}{\beta_f^3} (1 - \beta_f^2), \\ F_5^{z_f} &= \int_{-z_f}^{z_f} dc_\theta s_\theta^2 f^2(\theta) = \frac{-(1 - \beta_f^2) z_f}{\beta_f^2 (1 - z_f^2 \beta_f^2)} + \frac{\ln \frac{1+z_f\beta_f}{1-z_f\beta_f}}{2\beta_f^3} (1 + \beta_f^2). \end{aligned}$$

Then, all the 18 cross sections  $\hat{\Sigma}^X$  and  $\hat{\Delta}^X$  can be written in terms of  $\mathcal{W}_\sigma$ ,  $\mathcal{X}_\sigma$ ,  $\mathcal{Y}_{\sigma\lambda}$ , and  $\mathcal{Z}_{\sigma\lambda}$ . For example, the total cross section  $\hat{\Sigma}^{A_1}$  is

$$\hat{\Sigma}^{A_1} = \frac{\beta_f N_C}{32\pi} \left( \frac{\alpha m_f}{4\pi v^2} \right)^2 \frac{(\mathcal{Y}_{++} + \mathcal{Y}_{+-} + 2\mathcal{W}_+) + (\mathcal{Y}_{-+} + \mathcal{Y}_{--} + 2\mathcal{W}_-)}{4}, \quad (2.27)$$

and the other analogous quantities are given in the second column of Table 1.

The CP and CPT parities of the various cross sections are also shown in the first column of Table 1. The CP and CPT parities of the polarization-dependent cross sections can easily be obtained by observing that

$$\begin{aligned} \mathcal{W}_\sigma &\stackrel{\text{CP}}{\leftrightarrow} \mathcal{W}_{-\sigma}, \quad \mathcal{X}_\sigma &\stackrel{\text{CP}}{\leftrightarrow} \mathcal{X}_{-\sigma}^*, \quad \mathcal{Y}_{\sigma\lambda} &\stackrel{\text{CP}}{\leftrightarrow} \mathcal{Y}_{-\sigma-\lambda}, \quad \mathcal{Z}_{\sigma\lambda} &\stackrel{\text{CP}}{\leftrightarrow} \mathcal{Z}_{-\sigma-\lambda}, \\ \mathcal{W}_\sigma &\stackrel{\text{CPT}}{\leftrightarrow} \mathcal{W}_{-\sigma}, \quad \mathcal{X}_\sigma &\stackrel{\text{CPT}}{\leftrightarrow} \mathcal{X}_{-\sigma}, \quad \mathcal{Y}_{\sigma\lambda} &\stackrel{\text{CPT}}{\leftrightarrow} \mathcal{Y}_{-\sigma-\lambda}, \quad \mathcal{Z}_{\sigma\lambda} &\stackrel{\text{CPT}}{\leftrightarrow} \mathcal{Z}_{-\sigma-\lambda}^*, \end{aligned} \quad (2.28)$$

which are derived from (2.7) and (2.8). We observe that the half of the cross sections are CP odd.

## 2.5 Case III: Identical photon helicities

In this case, there are two possible initial-state photon helicity states to consider, so the amplitude again becomes a matrix:

$$\left( \mathcal{M}_\lambda^{\text{III}} \right)_{\sigma\bar{\sigma}} = \frac{\alpha m_f \sqrt{\hat{s}}}{4\pi v^2} \begin{pmatrix} \langle +; \lambda \rangle & 0 \\ 0 & \langle -; \lambda \rangle \end{pmatrix}, \quad (2.29)$$

where  $\langle \pm; \lambda \rangle$  were also defined in (2.10).

The polarization density matrices for the two final-state fermions are

$$\bar{\rho} = \frac{1}{2} \begin{pmatrix} 1 + \bar{P}_L & -\bar{P}_T e^{i\bar{\alpha}} \\ -\bar{P}_T e^{-i\bar{\alpha}} & 1 - \bar{P}_L \end{pmatrix}, \quad \rho = \frac{1}{2} \begin{pmatrix} 1 + P_L & P_T e^{-i\alpha} \\ P_T e^{i\alpha} & 1 - P_L \end{pmatrix}. \quad (2.30)$$

Here,  $P_L$  and  $\bar{P}_L$  are the longitudinal polarizations of the fermion  $f$  and antifermion  $\bar{f}$ , respectively, while  $P_T$  and  $\bar{P}_T$  are the degrees of transverse polarization with  $\alpha$  and  $\bar{\alpha}$  being the azimuthal angles with respect to the production plane. The polarization-weighted squared matrix elements are [37]

$$|\mathcal{M}_\lambda^{\text{III}}|^2 = \text{Tr} \left[ \mathcal{M}_\lambda^{\text{III}} \bar{\rho}^T \mathcal{M}_\lambda^{\text{III}\dagger} \rho \right]. \quad (2.31)$$

The total helicity-averaged cross section is obtained by summing over  $P$ ,  $\bar{P}$  and  $\lambda$  and dividing by a factor 4 to account for the initial-state spin average:

$$|\mathcal{M}_\lambda^{\text{III}}|^2 = \left( \frac{\alpha m_f \sqrt{\hat{s}}}{4\pi v^2} \right)^2 \left\{ D_1^\lambda (1 + P_L \bar{P}_L) + D_2^\lambda (P_L + \bar{P}_L) \right. \\ \left. + P_T \bar{P}_T [D_3^\lambda \cos(\alpha - \bar{\alpha}) + D_4^\lambda \sin(\alpha - \bar{\alpha})] \right\}, \quad (2.32)$$

where

$$D_1^\lambda = \frac{1}{4} (|\langle +; \lambda \rangle|^2 + |\langle -; \lambda \rangle|^2), \\ D_2^\lambda = \frac{1}{4} (|\langle +; \lambda \rangle|^2 - |\langle -; \lambda \rangle|^2), \\ D_3^\lambda = -\frac{1}{2} \Re (\langle +; \lambda \rangle \langle -; \lambda \rangle^*), \\ D_4^\lambda = \frac{1}{2} \Im (\langle +; \lambda \rangle \langle -; \lambda \rangle^*). \quad (2.33)$$

The quantities  $D_{3,4}^\lambda$  are related to the observables coming from the interference between the amplitudes with different fermion helicities, for which we need to measure the transverse polarizations of the final fermions. Note that the quantity  $D_1^\lambda$  can be constructed without the need to measure the helicities of the final fermions.

Similarly to the previous case, we define two kinds of cross sections, corresponding to the different initial-state photon helicities  $\lambda$ :

$$\frac{d\hat{\Sigma}^{D_i}}{dc_\theta} \equiv \frac{\beta_f N_C}{32\pi} \left( \frac{\alpha m_f}{4\pi v^2} \right)^2 (D_i^+ + D_i^-), \\ \frac{d\hat{\Delta}^{D_i}}{dc_\theta} \equiv \frac{\beta_f N_C}{32\pi} \left( \frac{\alpha m_f}{4\pi v^2} \right)^2 (D_i^+ - D_i^-). \quad (2.34)$$

Upon angle integration, we define

$$\widetilde{\mathcal{X}}_\lambda \equiv \int_{-z_f}^{z_f} dc_\theta \langle +; \lambda \rangle \langle -; \lambda \rangle^* = 2 \langle +; \lambda \rangle_H \langle -; \lambda \rangle_H^* + 2R(\hat{s})^2 F_1^{z_f} \langle +; \lambda \rangle_C \langle -; \lambda \rangle_C^* \\ + R(\hat{s}) F_2^{z_f} (\langle +; \lambda \rangle_C \langle -; \lambda \rangle_H^* + \langle +; \lambda \rangle_H \langle -; \lambda \rangle_C^*), \quad (2.35)$$

which satisfies

$$\tilde{\mathcal{X}}_\lambda \stackrel{\text{CP}}{\leftrightarrow} \tilde{\mathcal{X}}_{-\lambda}^*, \quad \tilde{\mathcal{X}}_\lambda \stackrel{\text{CPT}}{\leftrightarrow} \tilde{\mathcal{X}}_{-\lambda}. \quad (2.36)$$

Expressions for the cross sections  $\hat{\Sigma}^{D_i}$  and  $\hat{\Delta}^{D_i}$  after integrating over  $c_\theta$ , together with the CP and CPT parities of the cross sections, are given in Table 1. We, again, notice that the half of them are CP odd.

We complete this section by noting some relations between the cross sections, derived from the analytic expressions given above:

$$\begin{aligned} \hat{\sigma} &= \hat{\Sigma}^{A_1} - \hat{\Sigma}^{A_2} = \hat{\Sigma}^{D_1}, \\ (\hat{\Delta}_1 - \hat{\Delta}_2)/4 &= \hat{\Sigma}^{B_1} = \hat{\Delta}^{D_1}, \\ (\hat{\Delta}_1 + \hat{\Delta}_2)/4 &= \hat{\Delta}^{A_1} = \hat{\Sigma}^{D_2}, \\ \hat{\Delta}^{B_1} &= \hat{\Delta}^{D_2}. \end{aligned} \quad (2.37)$$

### 3 CP Violation in $\gamma\gamma \rightarrow \bar{b}b, \mu^+\mu^-, \tau^+\tau^-$ in a Three-Way Mixing Scenario

We now present some numerical examples of CP-violating Higgs signatures in  $\mu^+\mu^-, \tau^+\tau^-$ , and  $\bar{b}b$  production at a  $\gamma\gamma$  collider. As already mentioned, these signatures may be enhanced at large  $\tan\beta$ , and three-way mixing is potentially important for small charged (and hence also neutral) Higgs-boson masses. Therefore, we present in this section some numerical analyses in a specific scenario in which all the three neutral Higgs states mix significantly.

Explicitly, we take the following parameter set:

$$\begin{aligned} \tan\beta &= 50, \quad M_{H^\pm}^{\text{pole}} = 155 \text{ GeV}, \\ M_{\tilde{Q}_3} &= M_{\tilde{U}_3} = M_{\tilde{D}_3} = M_{\tilde{L}_3} = M_{\tilde{E}_3} = M_{\text{SUSY}} = 0.5 \text{ TeV}, \\ |\mu| &= 0.5 \text{ TeV}, \quad |A_{t,b,\tau}| = 1 \text{ TeV}, \quad |M_2| = |M_1| = 0.3 \text{ TeV}, \quad |M_3| = 1 \text{ TeV}, \\ \Phi_\mu &= 0^\circ, \quad \Phi_A = \Phi_{A_t} = \Phi_{A_b} = \Phi_{A_\tau} = 90^\circ, \quad \Phi_1 = \Phi_2 = 0^\circ, \end{aligned} \quad (3.1)$$

and we consider the following value for the phase of the gluino mass parameter  $M_3$ :  $\Phi_3 = -10^\circ$ . In this case, CPsuperH yields for the masses and widths of the neutral Higgs bosons:

$$\begin{aligned} M_{H_1} &= 120.2 \text{ GeV}, \quad M_{H_2} = 121.4 \text{ GeV}, \quad M_{H_3} = 124.5 \text{ GeV}, \\ \Gamma_{H_1} &= 1.19 \text{ GeV}, \quad \Gamma_{H_2} = 3.42 \text{ GeV}, \quad \Gamma_{H_3} = 3.20 \text{ GeV}. \end{aligned} \quad (3.2)$$

We present results for each of the above polarization cases in turn.

### 3.1 CP violation in $\gamma\gamma \rightarrow b\bar{b}$

In the process  $\gamma\gamma \rightarrow b\bar{b}$ , the inability of measuring the polarization of  $b$  and  $\bar{b}$  quarks limits us to two observables: the CP-even total helicity-averaged cross section  $\hat{\sigma}$  and the CP-odd cross section  $\hat{\Delta}_1 - \hat{\Delta}_2$ .

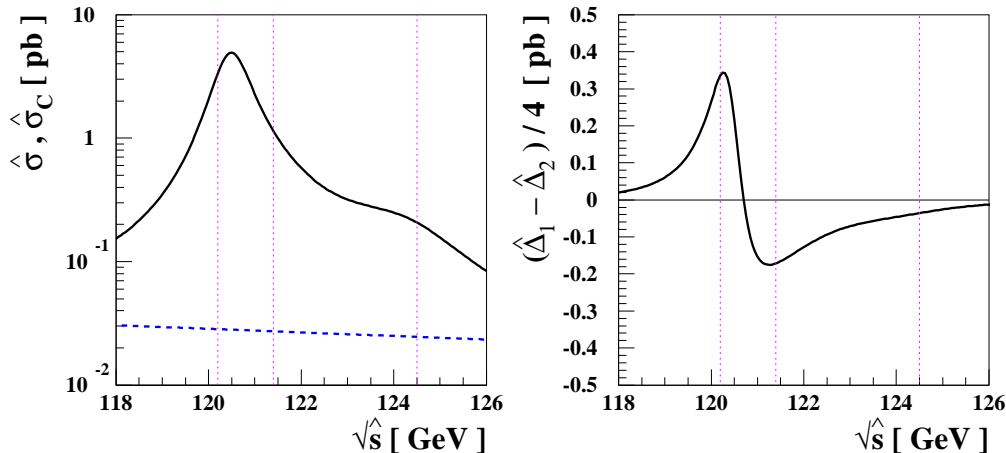


**Figure 3:** The cross sections  $\hat{\sigma}$  and  $(\hat{\Delta}_1 - \hat{\Delta}_2)/4$  for the process  $\gamma\gamma \rightarrow b\bar{b}$  in the three-way mixing scenario with  $\Phi_3 = -10^\circ$  and  $\Phi_{A_{t,b}} = 90^\circ$  as functions of  $\sqrt{\hat{s}}$  taking  $\theta_{\text{cut}}^b = 280$  mrad ( $z_b \simeq 0.96$ ). The continuum cross section  $\hat{\sigma}_C$  is also shown in the left frame as a dashed line. The three Higgs masses are indicated by vertical lines.

In Fig. 3, we show the cross sections as functions of the invariant mass of the bottom quarks  $\sqrt{\hat{s}}$  taking  $\theta_{\text{cut}}^b = 280$  mrad ( $z_b \simeq 0.96$ ) coming from the coverage of the vertex detector. In the left frame, we also show the QED continuum cross section  $\hat{\sigma}_C$  as a dashed line. We observe the continuum contribution to the total cross section is negligible taking account of  $\theta_{\text{cut}}^b = 280$  mrad. The total helicity-averaged cross section is larger than about  $\sim 0.1$  pb in the region shown except around  $\sqrt{\hat{s}} = 126$  GeV. The maximum center-of-mass energy and the luminosity in  $\gamma\gamma$  collisions are comparable to those in  $e^\pm e^-$  collisions [38]. Assuming an integrated  $\gamma\gamma$  luminosity of  $100 \text{ fb}^{-1}$ , and high efficiency for  $b$ -quark reconstruction, we may expect a sample exceeding ten thousand events. This would enable one to probe CP asymmetry at the 1 % level or less in the process  $\gamma\gamma \rightarrow b\bar{b}$ , by controlling the polarizations of colliding photon beams.

The CP-violating cross section  $(\hat{\Delta}_1 - \hat{\Delta}_2)/4$  is in a range between  $-0.2$  pb and  $0.3$  pb. We define a CP asymmetry as:

$$\mathcal{A}_0 \equiv \frac{\hat{\Delta}_1 - \hat{\Delta}_2}{4 \hat{\sigma}}. \quad (3.3)$$

In Fig. 4, we show this CP asymmetry as a function of  $\sqrt{\hat{s}}$ . We observe that  $|\mathcal{A}_0|$  is larger than 1 % over most of the region and can be as large as 25 %.

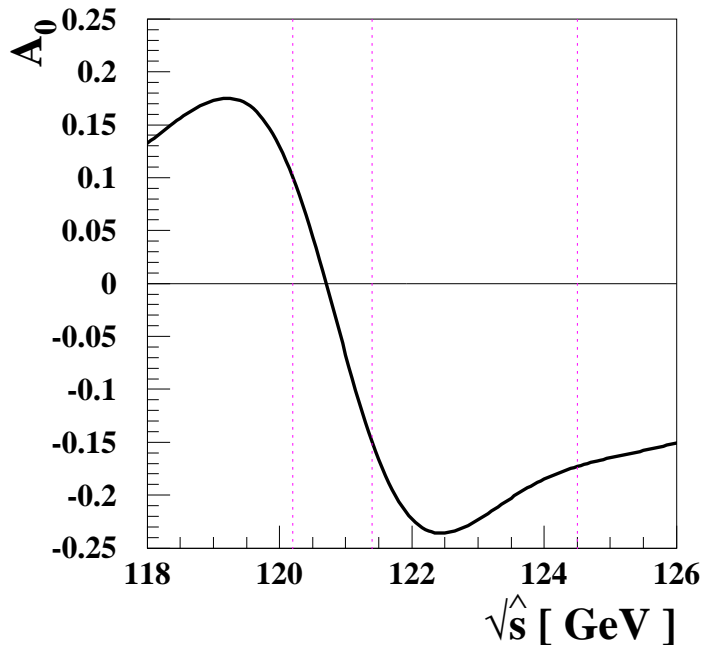


**Figure 4:** The CP asymmetry  $\mathcal{A}_0$  for the process  $\gamma\gamma \rightarrow \bar{b}b$  in the three-way mixing scenario with  $\Phi_3 = -10^\circ$  and  $\Phi_{A_{t,b}} = 90^\circ$ , as a function of  $\sqrt{\hat{s}}$  taking  $\theta_{\text{cut}}^b = 280$  mrad ( $z_b \simeq 0.96$ ).

On the other hand, it should be noted that the  $\bar{b}b$  mass resolution in a realistic detector at a  $\gamma\gamma$  collider is expected to be several GeV [39], in which case the regions of positive and negative  $\mathcal{A}_0$  would be somewhat smeared. However, at least in this example, the integrated asymmetry should still be non-zero and observable. Nevertheless, this physics example indicates that some premium should be set on a detector capable of good  $\bar{b}b$  mass resolution.

### 3.2 CP violation in $\gamma\gamma \rightarrow \mu^+\mu^-$

In this process, as in the process  $\gamma\gamma \rightarrow \bar{b}b$ , the inability to measure the polarization of muons limits us to two observables: the CP-even total helicity-averaged cross section  $\hat{\sigma}$  and the CP-odd cross section  $(\hat{\Delta}_1 - \hat{\Delta}_2)/4$ . But, differently from the  $\gamma\gamma \rightarrow \bar{b}b$  process, the good resolution in the invariant mass of the muons, which is expected to be better than 1 GeV, enables us to examine the  $\sqrt{\hat{s}}$  dependence of the cross sections and the CP asymmetry in the process  $\gamma\gamma \rightarrow \mu^+\mu^-$ .

In Figs. 5 and 6, we show the cross sections  $\hat{\sigma}$  and  $(\hat{\Delta}_1 - \hat{\Delta}_2)/4$  and the CP asymmetry  $\mathcal{A}_0$ . The angle cut  $\theta_{\text{cut}}^\mu = 130$  mrad, which corresponds to  $z_\mu \simeq 0.99$ , has been taken. The cross section  $\hat{\sigma}$  is larger than  $\sim 4$  fb and the CP asymmetry can be as large as 20 %. With  $100 \text{ fb}^{-1}$  integrated  $\gamma\gamma$  luminosity, we expect to have a sample of a few hundred events which is enough to probe a CP asymmetry larger than 10 %.

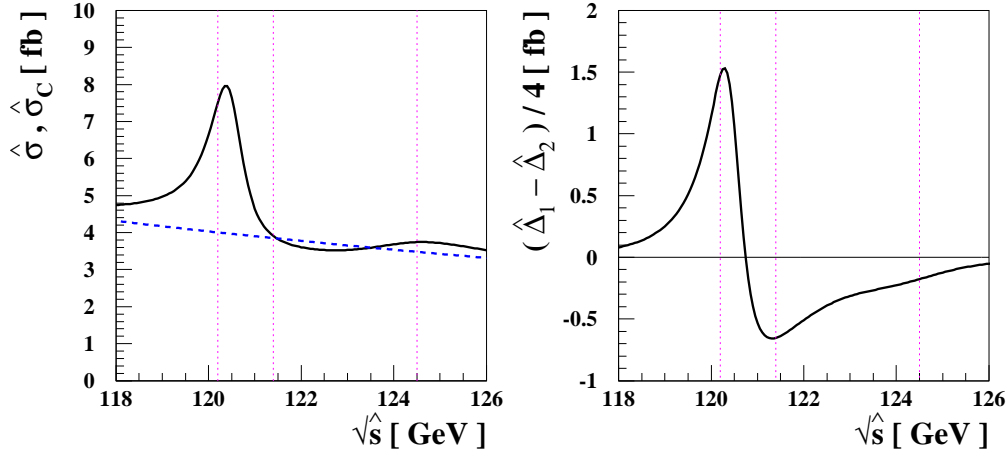


**Figure 5:** The cross sections  $\hat{\sigma}$  and  $(\hat{\Delta}_1 - \hat{\Delta}_2)/4$  for the process  $\gamma\gamma \rightarrow \mu^+\mu^-$  in the three-way mixing scenario with  $\Phi_3 = -10^\circ$  and  $\Phi_{A_{t,b}} = 90^\circ$ , as functions of  $\sqrt{\hat{s}}$  with  $\theta_{\text{cut}}^\mu = 130$  mrad ( $z_\mu \simeq 0.99$ ). The continuum cross section  $\hat{\sigma}_C$  is also shown in the left frame as a dashed line. The three Higgs masses are indicated by vertical lines.

### 3.3 CP violation in $\gamma\gamma \rightarrow \tau^+\tau^-$

In this subsection, we consider all the observables introduced in Sec. 2, since the polarizations of tau leptons can be measured in the process  $\gamma\gamma \rightarrow \tau^+\tau^-$  [32]. For the process, we impose  $\theta_{\text{cut}}^\tau = 130$  mrad ( $z_\tau \simeq 0.99$ ) which is the same as  $\theta_{\text{cut}}^\mu$ . We find that the CP-even cross sections  $\hat{\sigma}$ ,  $\hat{\Sigma}^{A_1}$ ,  $\hat{\Delta}^{B_1}$ ,  $\hat{\Sigma}^{D_1}$ , and  $\hat{\Delta}^{D_2}$ , which are expressed in terms of  $\mathcal{Y}_{\sigma\lambda}$ , are very sensitive to the value of  $\theta_{\text{cut}}^\mu$ . But the other observables are nearly insensitive as long as  $(1 - z_\tau) \ll 1$ .

In Fig. 7, we show the cross sections for Case I (identical photon and fermion helicities) as functions of the invariant mass of the tau leptons in the three-way mixing scenario. The upper two frames are for  $\hat{\sigma}_{\sigma\lambda}$ . When  $\sigma = \lambda$  (upper-left frame), the cross sections are around 2-5 pb and the contribution from the QED continuum is comparable to that from the Higgs-mediated process around  $\sqrt{\hat{s}} = 120$  GeV, as seen from  $\hat{\sigma}_C$  (dashed line) in the lower-left frame. We observe the sizable difference between  $\hat{\sigma}_{++}$  and  $\hat{\sigma}_{--}$ , which is just the

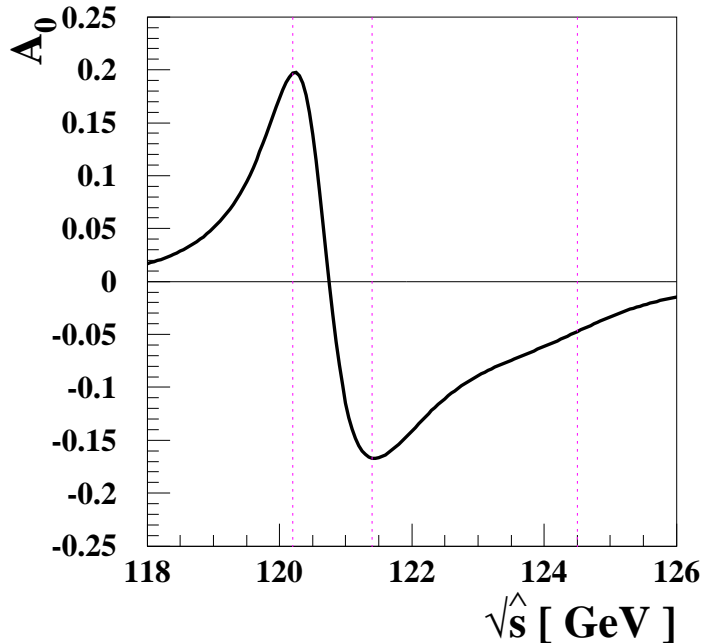


**Figure 6:** The CP asymmetry  $\mathcal{A}_0$  for the process  $\gamma\gamma \rightarrow \mu^+\mu^-$  in the three-way mixing scenario with  $\Phi_3 = -10^\circ$  and  $\Phi_{A_{t,b}} = 90^\circ$ , as a function of  $\sqrt{\hat{s}}$  with  $\theta_{\text{cut}}^\mu = 130$  mrad.

$\hat{\Delta}_1$  shown as a solid line in the lower-right frame. When  $\sigma \neq \lambda$  (upper-right frame), the cross sections are peaked between  $M_{H_1}$  and  $M_{H_2}$  with sizes of about 2 pb ( $\hat{\sigma}_{+-}$ ) and 0.5 pb ( $\hat{\sigma}_{-+}$ ) as shown by solid and dashed lines, respectively. In this case the contribution from the QED continuum is negligible since the amplitude is suppressed by the factor  $(1 - \beta_\tau)$ , see Eq. (2.11). Again we see a sizable difference between the two cross sections, which is the CP-violating cross section  $\hat{\Delta}_2$  shown in the frame below as a dashed line.

We show in Fig. 8 the CP asymmetries defined by

$$\mathcal{A}_1 \equiv \frac{\hat{\Delta}_1}{\hat{\sigma}_{++} + \hat{\sigma}_{--}}, \quad \mathcal{A}_2 \equiv \frac{\hat{\Delta}_2}{\hat{\sigma}_{+-} + \hat{\sigma}_{-+}}. \quad (3.4)$$

The CP asymmetry  $\mathcal{A}_1$  is larger than 10 % in the region  $\sqrt{\hat{s}} \sim M_{H_1}$ . Assuming 10,000  $\gamma\gamma \rightarrow \tau^+\tau^-$  events after some experimental cuts to reconstruct the tau leptons and their polarizations, CP asymmetries larger than 1 % could be measured. The intrinsic CP asymmetry  $\mathcal{A}_2$  is larger than 10 % in the whole region and can be as large as 70 %. Between  $\sqrt{\hat{s}} = M_{H_1}$  and  $M_{H_2}$  where the sum of the cross sections  $\hat{\sigma}_{+-} + \hat{\sigma}_{-+}$  is larger than 1 pb, the asymmetry is larger than 50 %. However, the  $\tau^+\tau^-$  mass resolution is expected,



realistically, to be larger than that for  $\bar{b}b$  final states, so that these fine details would be washed out and only asymmetries integrated over the resonance peaks would be observable.

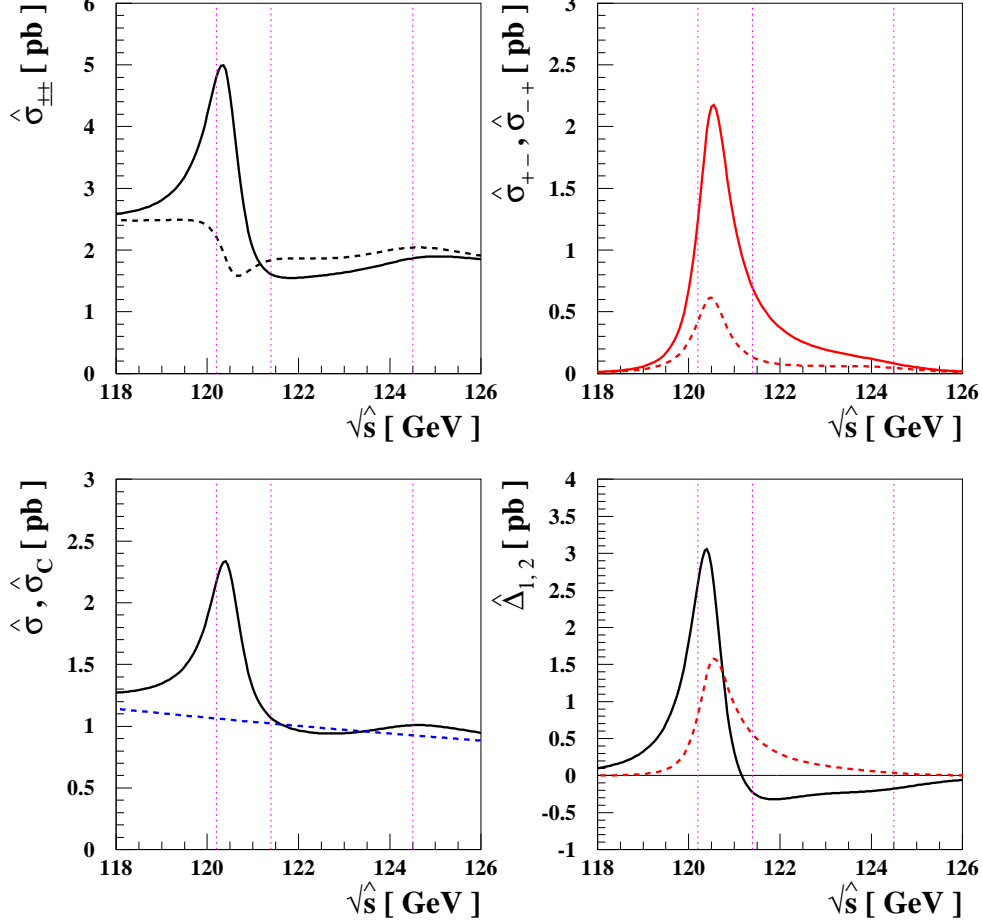


**Figure 7:** The cross sections for the process  $\gamma(\lambda)\gamma(\lambda) \rightarrow \tau^+(\sigma)\tau^-(\sigma)$  (Case I) in the three-way mixing scenario with  $\Phi_3 = -10^\circ$  and  $\Phi_{A_t,b} = 90^\circ$ , as functions of  $\sqrt{\hat{s}}$ . In panels (a, b, c) and (d), the solid lines are for  $\hat{\sigma}_{++}$ ,  $\hat{\sigma}_{+-}$ ,  $\hat{\sigma}$  and  $\hat{\Delta}_1$ , and the dashed lines for  $\hat{\sigma}_{--}$ ,  $\hat{\sigma}_{-+}$ , the continuum cross section  $\hat{\sigma}_C$  and  $\hat{\Delta}_2$ , respectively. The three Higgs masses are indicated by vertical lines.

Figs. 9 and 10 display the cross sections  $\hat{\Sigma}^{A_i,B_j,C_k}(\gamma\gamma \rightarrow \tau^+\tau^-)$  and  $\hat{\Delta}^{A_i,B_j,C_k}(\gamma\gamma \rightarrow \tau^+\tau^-)$ , respectively, in the three-way mixing scenario. The CP-odd cross sections are shown with dashed lines. Note that  $\hat{\Sigma}^{A_2}$  and all the observables related with  $C_i$  ( $\hat{\Sigma}^{C_k}$  and  $\hat{\Delta}^{C_k}$  with  $k = 1, 2, 3, 4$ ) are one or two orders of magnitude smaller than other observables. We see that  $\hat{\Sigma}^{C_1}$  and  $\hat{\Sigma}^{C_4}$ , which are CP-odd, are too small to be observed. But the other CP-odd observables  $\hat{\Delta}^{A_1}$ ,  $\hat{\Sigma}^{B_1}$ ,  $\hat{\Sigma}^{B_2}$  and  $\hat{\Delta}^{B_3}$ , which are larger than 0.1 pb, may well be measurable.

Figs. 11 and 12 display the cross sections  $\hat{\Sigma}^{D_i}(\gamma\gamma \rightarrow \tau^+\tau^-)$  and  $\hat{\Delta}^{D_i}(\gamma\gamma \rightarrow \tau^+\tau^-)$ , respectively, in the three-way mixing scenario. Again, the CP-odd cross sections are indicated

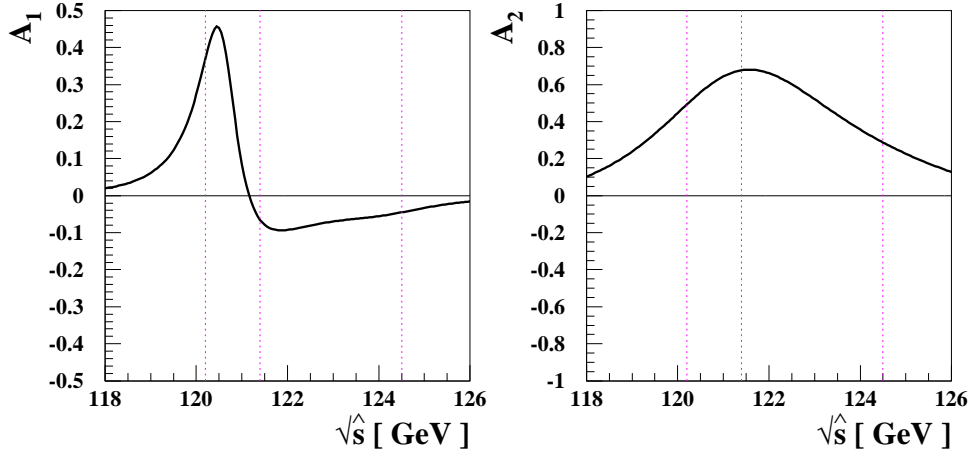


**Figure 8:** The CP asymmetries  $\mathcal{A}_1$  and  $\mathcal{A}_2$  for the process  $\gamma\gamma \rightarrow \tau^+\tau^-$  in the three-way mixing scenario with  $\Phi_3 = -10^\circ$  and  $\Phi_{A_{t,b}} = 90^\circ$ , as functions of  $\sqrt{\hat{s}}$ .

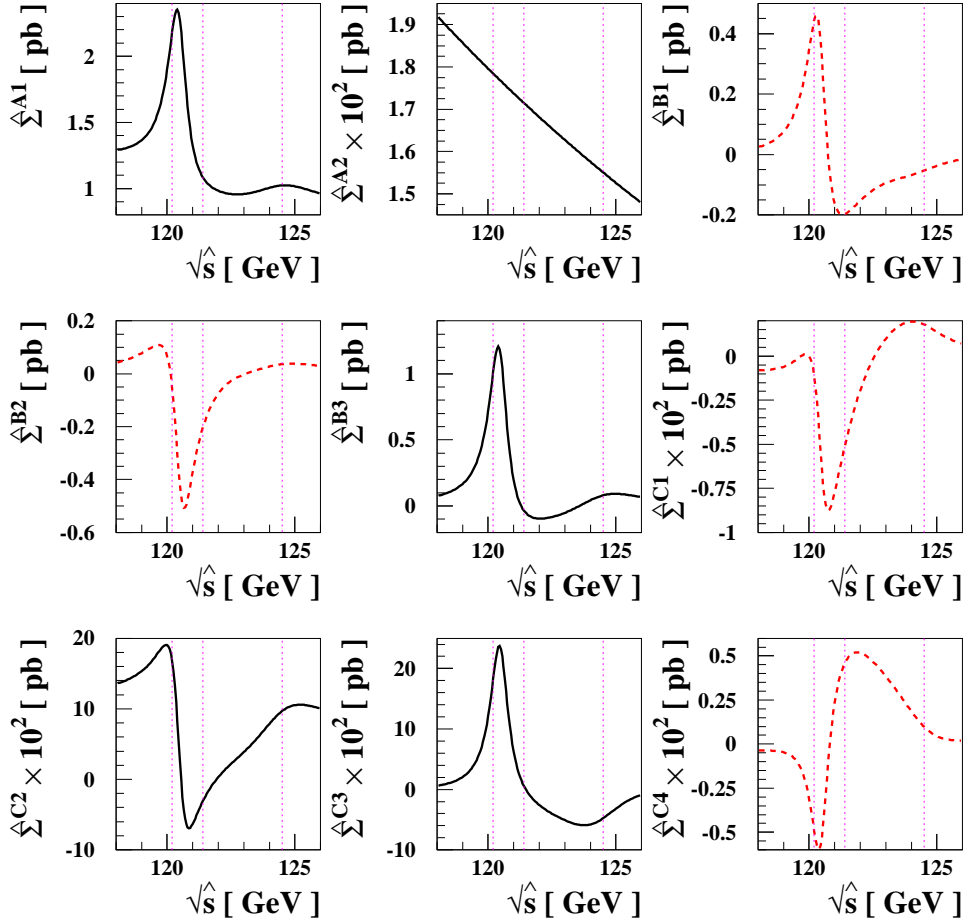


**Figure 9:** The cross sections  $\hat{\Sigma}^X$  for the process  $\gamma(\lambda_1)\gamma(\lambda_2) \rightarrow \tau^+(\sigma)\tau^-(\sigma)$  (Case II) in the three-way mixing scenario with  $\Phi_3 = -10^\circ$  and  $\Phi_{A_{t,b}} = 90^\circ$  as functions of  $\sqrt{\hat{s}}$ .

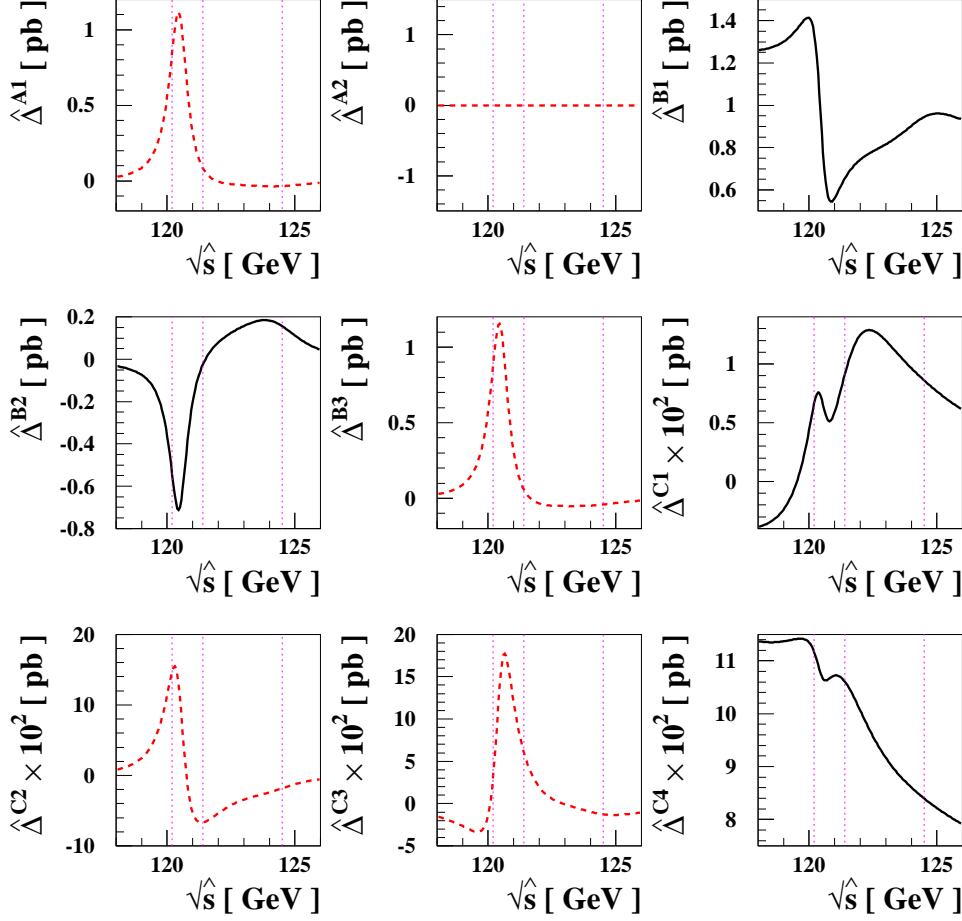


**Figure 10:** The cross sections  $\hat{\Delta}^X$  for the process  $\gamma(\lambda_1)\gamma(\lambda_2) \rightarrow \tau^+(\sigma)\tau^-(\sigma)$  (Case II) in the three-way mixing scenario with  $\Phi_3 = -10^\circ$  and  $\Phi_{A_{t,b}} = 90^\circ$  as functions of  $\sqrt{\hat{s}}$ .

by dashed lines. The CP-odd cross sections larger than 0.1 pb may well be measurable.

## 4 CP Violation in $\gamma\gamma \rightarrow \bar{t}t$ in a Two-Way Mixing Scenario

The formalism developed above applies equally well to the process  $\gamma\gamma \rightarrow \bar{t}t$  [31, 33, 40]. However, resonant  $\bar{t}t$  production is not possible in the scenario with strong three-way mixing that was presented previously. Hence, in order to exhibit the possible CP-violating signatures in  $\gamma\gamma \rightarrow \bar{t}t$ , we introduce a scenario with a heavier charged Higgs boson and strong two-way neutral-Higgs mixing.

The parameters are taken as:

$$\tan\beta = 10, \quad M_{H^\pm}^{\text{pole}} = 0.5 \text{ TeV}, \quad |\mu| = 1 \text{ TeV},$$

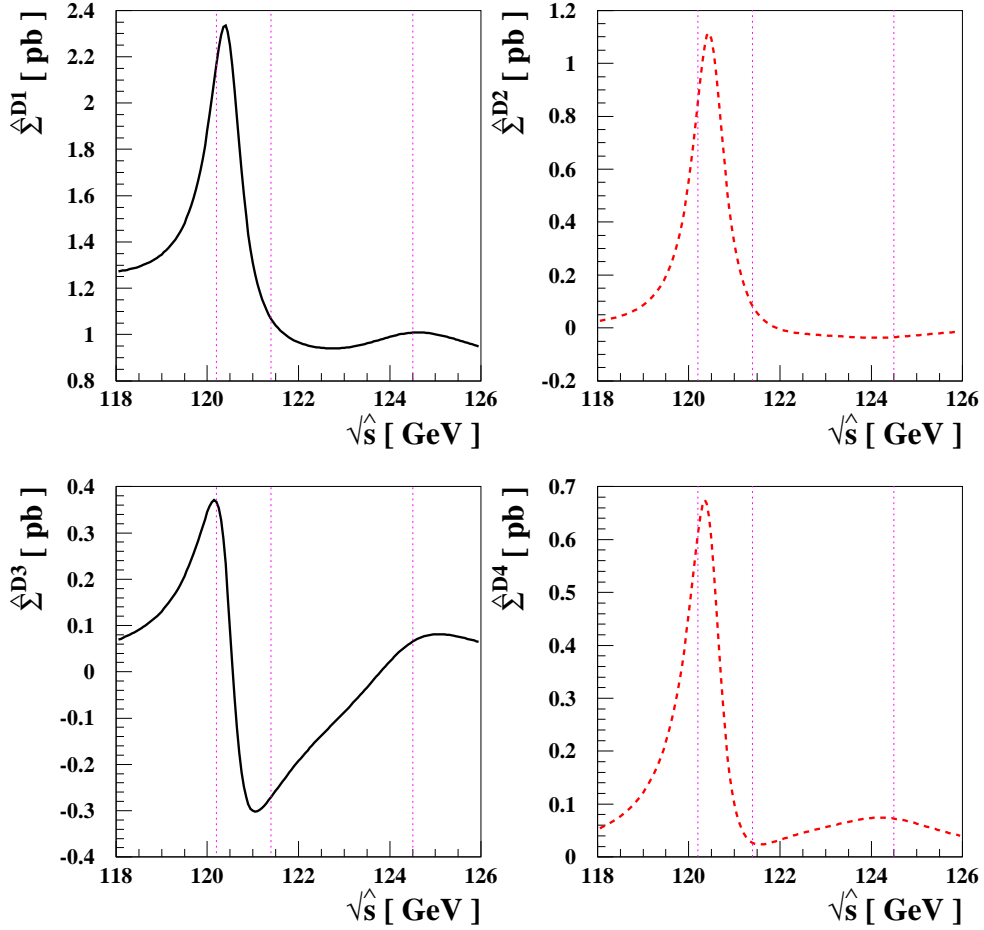


**Figure 11:** The cross sections  $\hat{\Sigma}^{D_i}$  for the process  $\gamma(\lambda)\gamma(\lambda) \rightarrow \tau^+(\bar{\sigma})\tau^-(\sigma)$  (Case III) in the three-way mixing scenario with  $\Phi_3 = -10^\circ$  and  $\Phi_{A_{t,b}} = 90^\circ$  as functions of  $\sqrt{\hat{s}}$ .

$$\begin{aligned}
 |M_3| &= 1 \text{ TeV}, \quad M_{\text{SUSY}} = 0.5 \text{ TeV}, \quad |A_{t,b}| = 1 \text{ TeV}, \\
 \Phi_{A_{t,b}} &= 90^\circ, \quad \Phi_3 = 180^\circ.
 \end{aligned}
 \tag{4.1}$$

In this scenario, the masses and widths of the heavier neutral Higgs bosons are

$$\begin{aligned}
 M_{H_2} &= 490.7 \text{ GeV}, \quad \Gamma_{H_2} = 2.036 \text{ GeV}, \\
 M_{H_3} &= 495.2 \text{ GeV}, \quad \Gamma_{H_2} = 1.969 \text{ GeV},
 \end{aligned}
 \tag{4.2}$$

with  $M_{H_1} = 121.0 \text{ GeV}$ .

In Fig. 13, we show the cross sections  $\hat{\sigma}_{\sigma\lambda}$ , the helicity-averaged cross section  $\hat{\sigma}$ , the QED continuum cross section  $\hat{\sigma}_C$ , and CP-violating cross section  $\hat{\Delta}_{1,2}$  as functions of the invariant mass of a top quark pair,  $\sqrt{\hat{s}}$ . The line conventions are the same as in Fig. 7. For  $\sigma = \lambda$ , the cross sections lie between 1.3 pb and 1.8 pb. The difference between two cross sections,  $\hat{\Delta}_1$ , is about 0.4 pb at  $\sqrt{\hat{s}} = M_{H_2}$ , but is much smaller at  $\sqrt{\hat{s}} = M_{H_3}$ , as shown in the lower-right frame. When  $\sigma \neq \lambda$ , the cross sections are about an order of

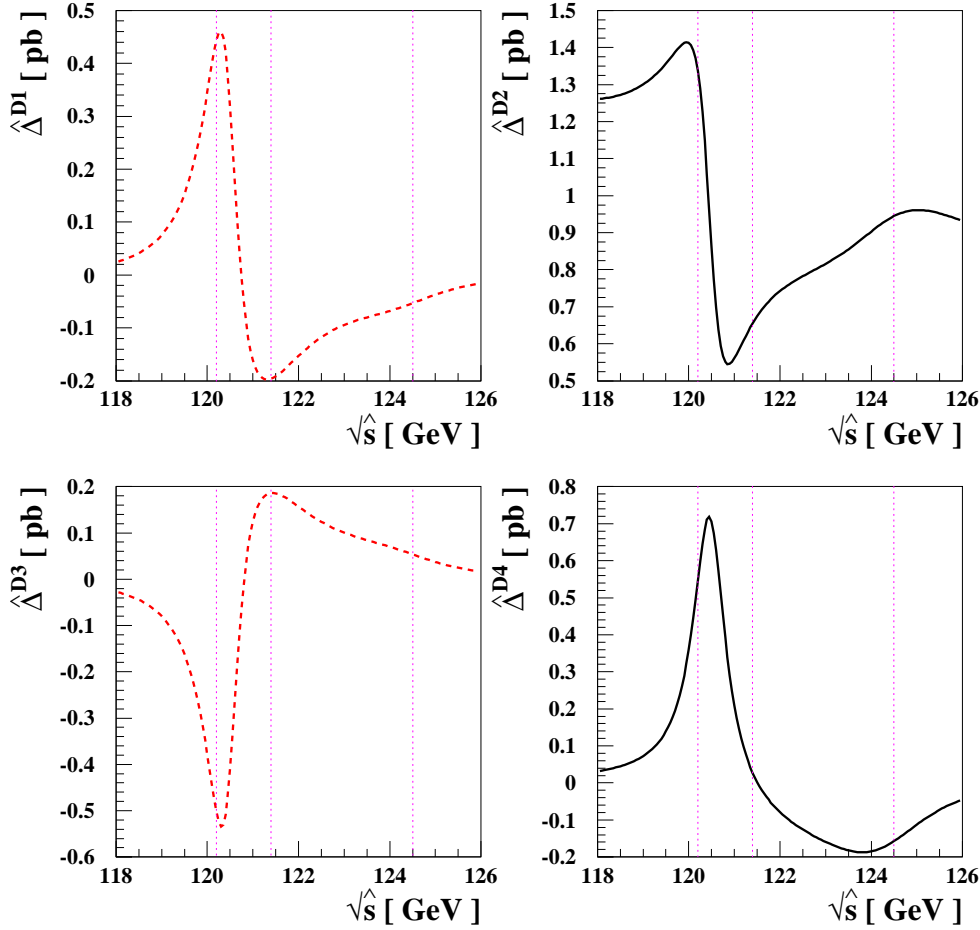


**Figure 12:** The cross sections  $\hat{\Delta}^{D_i}$  for the process  $\gamma(\lambda)\gamma(\lambda) \rightarrow \tau^+(\bar{\sigma})\tau^-(\sigma)$  (Case III) in the three-way mixing scenario with  $\Phi_3 = -10^\circ$  and  $\Phi_{A_{t,b}} = 90^\circ$  as functions of  $\sqrt{\hat{s}}$ .

magnitude smaller than those for the case  $\sigma = \lambda$ . The difference of the cross sections,  $\hat{\Delta}_2$ , could be as large as 0.1 pb at  $\sqrt{\hat{s}} = M_{H_2}$ . The cross sections may well be large enough to be measurable. Two CP asymmetries  $\mathcal{A}_{1,2}$  which are defined in (3.4), are shown in Fig. 14. We see large CP asymmetries only around the  $H_2$  Higgs-boson peak for the parameter set chosen.

In Figs. 15 and 16, the cross sections  $\hat{\Sigma}^{A_i, B_j, C_k}(\gamma\gamma \rightarrow t\bar{t})$  and  $\hat{\Delta}^{A_i, B_j, C_k}(\gamma\gamma \rightarrow t\bar{t})$  are shown, respectively. All the cross sections larger than 0.01 pb may well be measurable. Even the smallest CP-odd cross sections  $\hat{\Sigma}^{C_1}$  and  $\hat{\Sigma}^{C_4}$ , which are denoted by dashed lines, have a size of a few fb at  $\sqrt{\hat{s}} = M_{H_2}$  and  $M_{H_3}$ .

Figs. 17, and 18 display the cross sections  $\hat{\Sigma}^{D_i}(\gamma\gamma \rightarrow t\bar{t})$  and  $\hat{\Delta}^{D_i}(\gamma\gamma \rightarrow t\bar{t})$ , respectively, in the two-way mixing scenario. Again, the CP-odd cross sections are indicated by dashed lines, and the CP-odd cross sections are large enough to be measured.

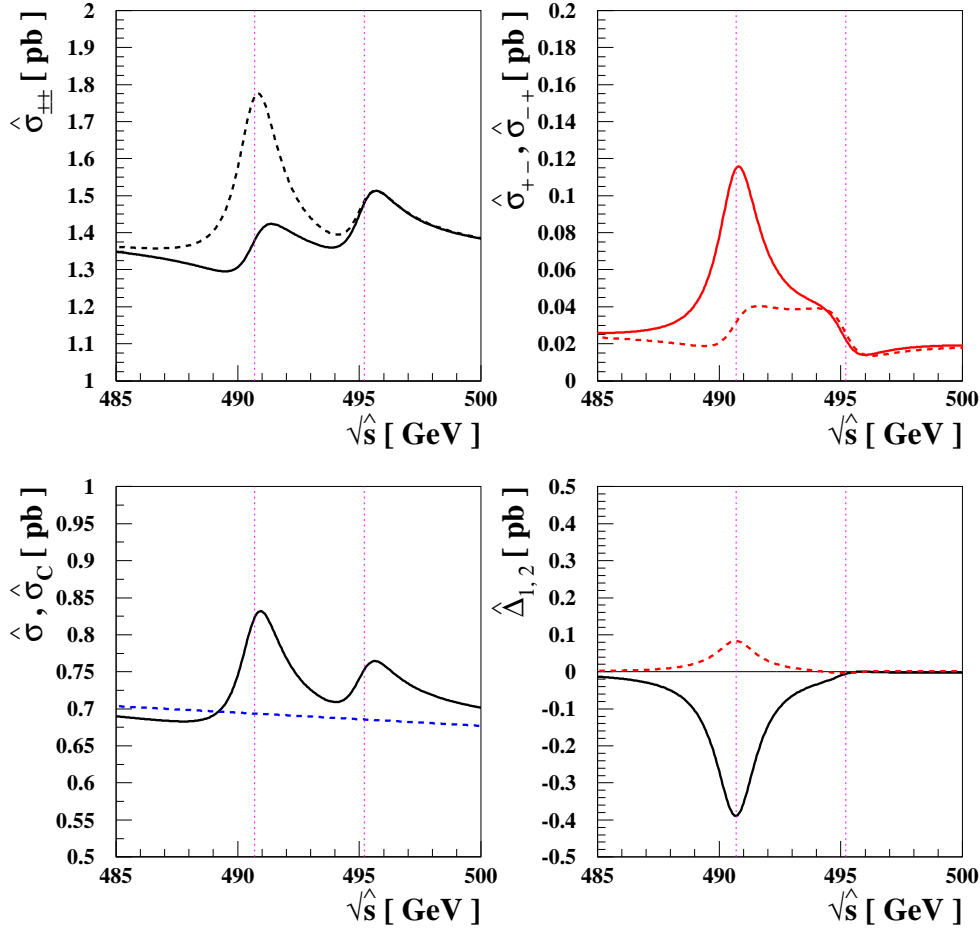


**Figure 13:** *The cross sections for the process  $\gamma(\lambda)\gamma(\lambda) \rightarrow t(\sigma)\bar{t}(\sigma)$  (Case I) as functions of  $\sqrt{\hat{s}}$ . The parameter set (4.1) is taken. The solid lines are for  $\hat{\sigma}_{++}$ ,  $\hat{\sigma}_{+-}$ ,  $\hat{\sigma}$ , and  $\hat{\Delta}_1$ , and the dashed lines for  $\hat{\sigma}_{--}$ ,  $\hat{\sigma}_{-+}$ , the continuum cross section  $\hat{\sigma}_C$ , and  $\hat{\Delta}_2$ . The heavier Higgs-boson masses are represented with vertical lines.*

## 5 Conclusions

There is general agreement that the CP violation contained in the Standard Model, though it is consistent with all the laboratory data available so far, is inadequate for generating the baryon asymmetry of the Universe. One of the most appealing scenarios for physics beyond the Standard Model that might yield sufficient supplementary CP violation is supersymmetry which reopens the possibility of baryogenesis at the electroweak scale [41]. Supersymmetric CP violation may appear directly both in sparticle production or decays and in the production and decays of MSSM Higgs bosons.

We presented previously a general formalism for analyzing CP-violating phenomena in the production, mixing and decay of a coupled system of multiple CP-violating neutral Higgs bosons, and applied it to Higgs production and decay at the LHC [21].

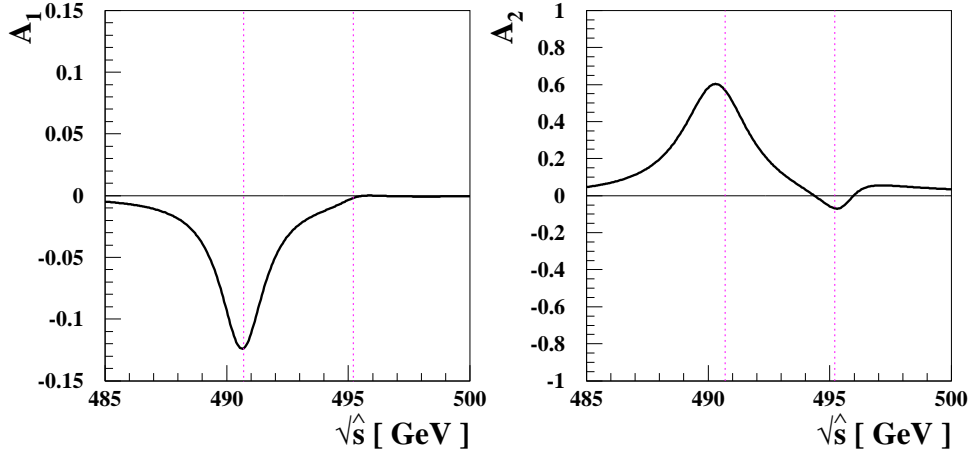


Figure 14: The CP asymmetries  $\mathcal{A}_1$  and  $\mathcal{A}_2$  for the process  $\gamma\gamma \rightarrow t\bar{t}$  in the two-way mixing scenario as functions of  $\sqrt{\hat{s}}$ .

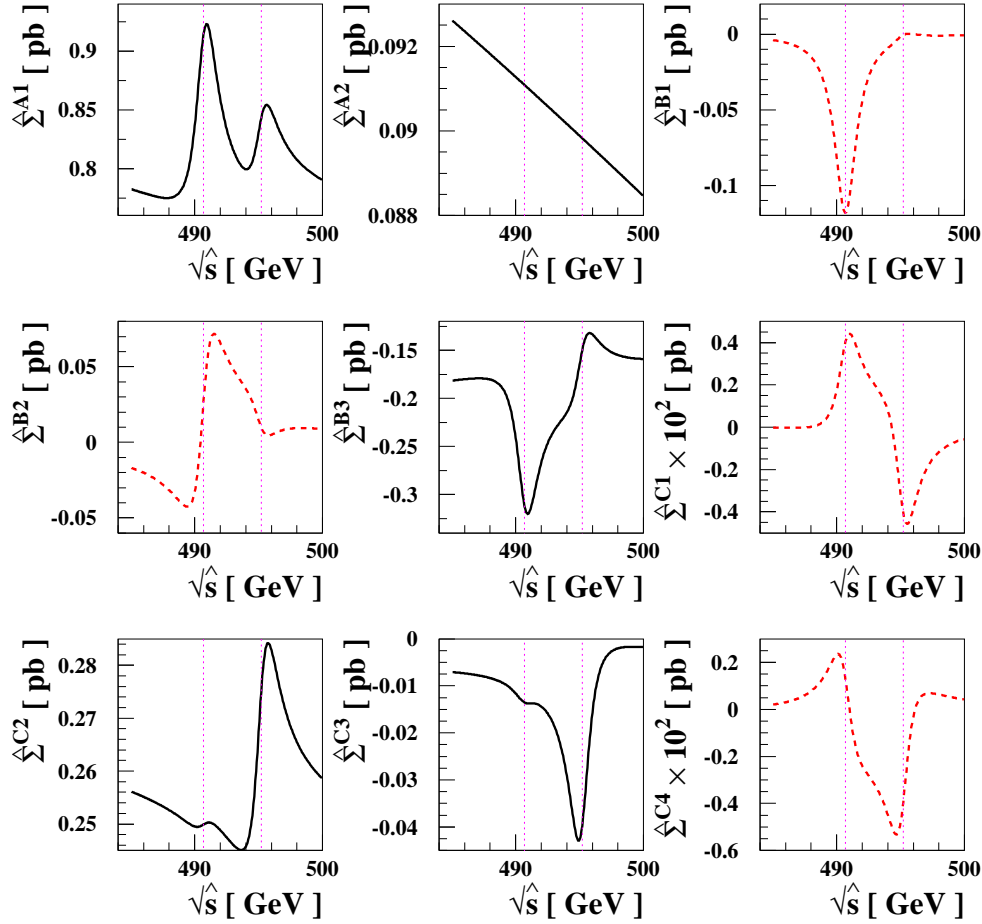
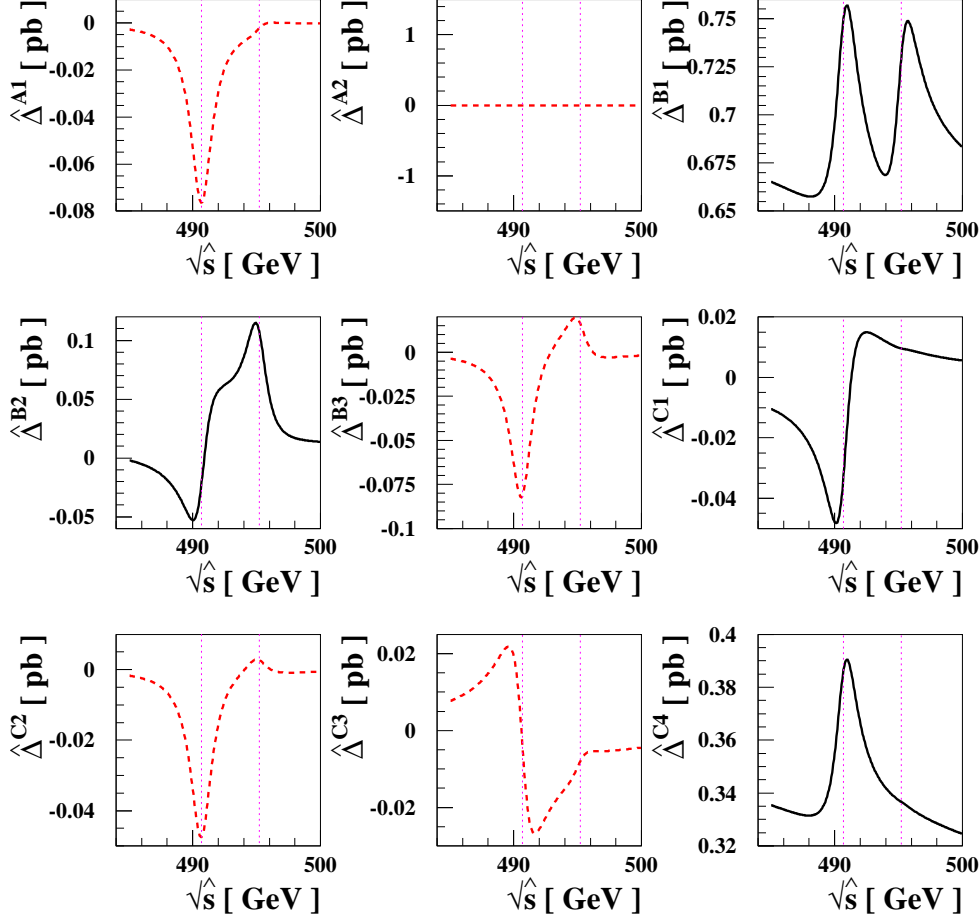


Figure 15: The cross sections  $\hat{\Sigma}^X(\gamma(\lambda_1)\gamma(\lambda_2) \rightarrow t(\sigma)\bar{t}(\sigma))$  (Case II) as functions of  $\sqrt{\hat{s}}$  for the parameter set (4.1).



**Figure 16:** The cross sections  $\hat{\Delta}^X(\gamma(\lambda_1)\gamma(\lambda_2) \rightarrow t(\sigma)\bar{t}(\sigma))$  (Case II) as functions of  $\sqrt{\hat{s}}$  for the parameter set (4.1).

In this paper, as a further application of this formalism, we have studied in detail the production and decays of CP-violating MSSM  $H_{1,2,3}$  bosons in  $\gamma\gamma$  collisions, studying  $\mu^+\mu^-$ ,  $\tau^+\tau^-$ ,  $\bar{b}b$  and  $\bar{t}t$  final states. We have constructed more than 20 independent observables by exploiting the controllable beam polarization at  $\gamma\gamma$  colliders and the possibly measurable final-fermion polarizations. We have classified them according to their CP and  $C\tilde{P}$  parities and note that the half of them are genuine CP-odd observables. We have considered two specific MSSM scenarios that predict either (a) three nearly degenerate, strongly-mixed Higgs bosons with  $M_{H_{1,2,3}} \sim 120$  GeV or (b) two nearly degenerate, strongly-mixed Higgs bosons with  $M_{H_{2,3}} \sim 490$  GeV. Some of the CP-violating signatures we have explored may be quite large, rising to 20 % in some cases. Particularly promising examples seem to be the asymmetry  $\mathcal{A}_0$  in  $\gamma\gamma \rightarrow \bar{b}b$  and  $\gamma\gamma \rightarrow \mu^+\mu^-$  in the three-way mixing scenario, and the asymmetries  $\mathcal{A}_1$  and  $\mathcal{A}_2$  for the processes  $\gamma\gamma \rightarrow \tau^+\tau^-$  in the three-way mixing scenario and  $\gamma\gamma \rightarrow \bar{t}t$  in the two-way mixing scenario. However, many other potential signatures may also be interesting.



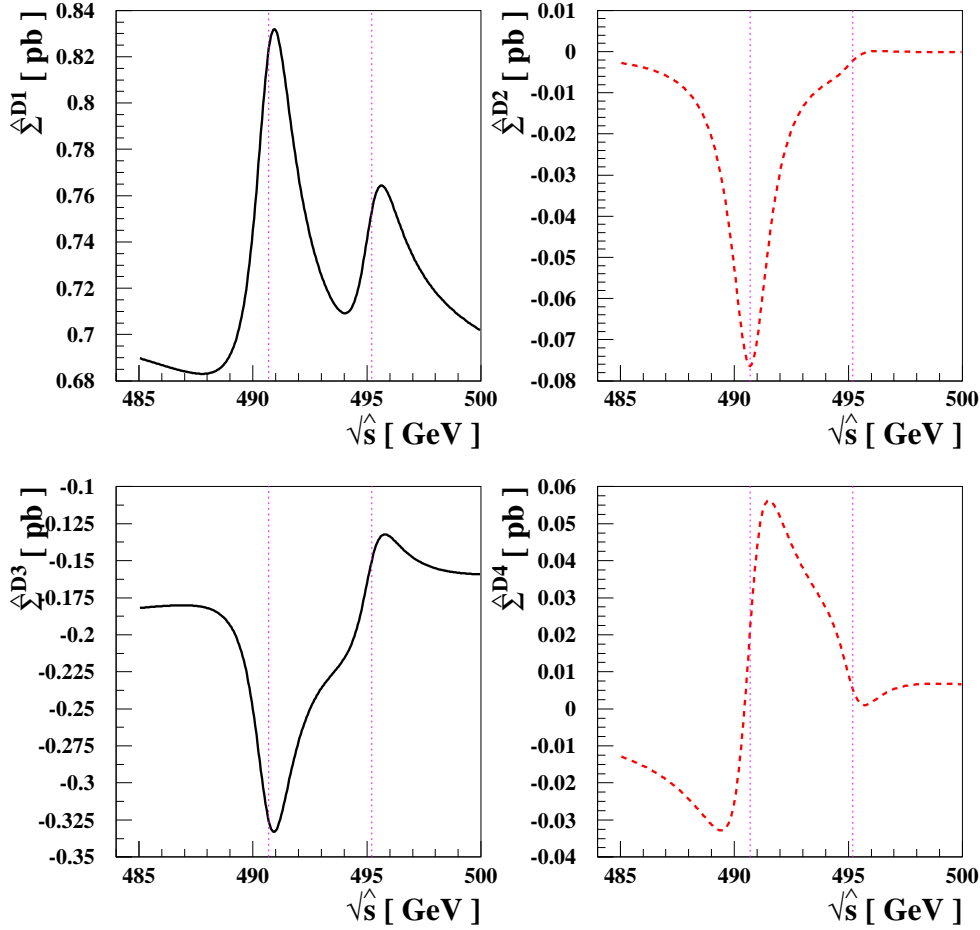


**Figure 17:** The cross sections  $\hat{\Sigma}^{D_i}(\gamma(\lambda)\gamma(\lambda) \rightarrow t(\sigma)\bar{t}(\bar{\sigma}))$  (Case III) for the parameter set (4.1) as functions of  $\sqrt{\hat{s}}$ .

Our study confirms that a  $\gamma\gamma$  collider would be a valuable tool for unravelling CP violation in the MSSM. In particular, the controllable initial-state polarizations offered by a  $\gamma\gamma$  collider could provide sensitive tools for unravelling the origin of CP violation and, by extension, the possibility of electroweak baryogenesis.

## Acknowledgements

We thank Klaus Desch for valuable advice on experimental parameters relevant for this study. The work of JSL and AP is supported in part by the PPARC research grant PPA/G/O/ 2000/00461.

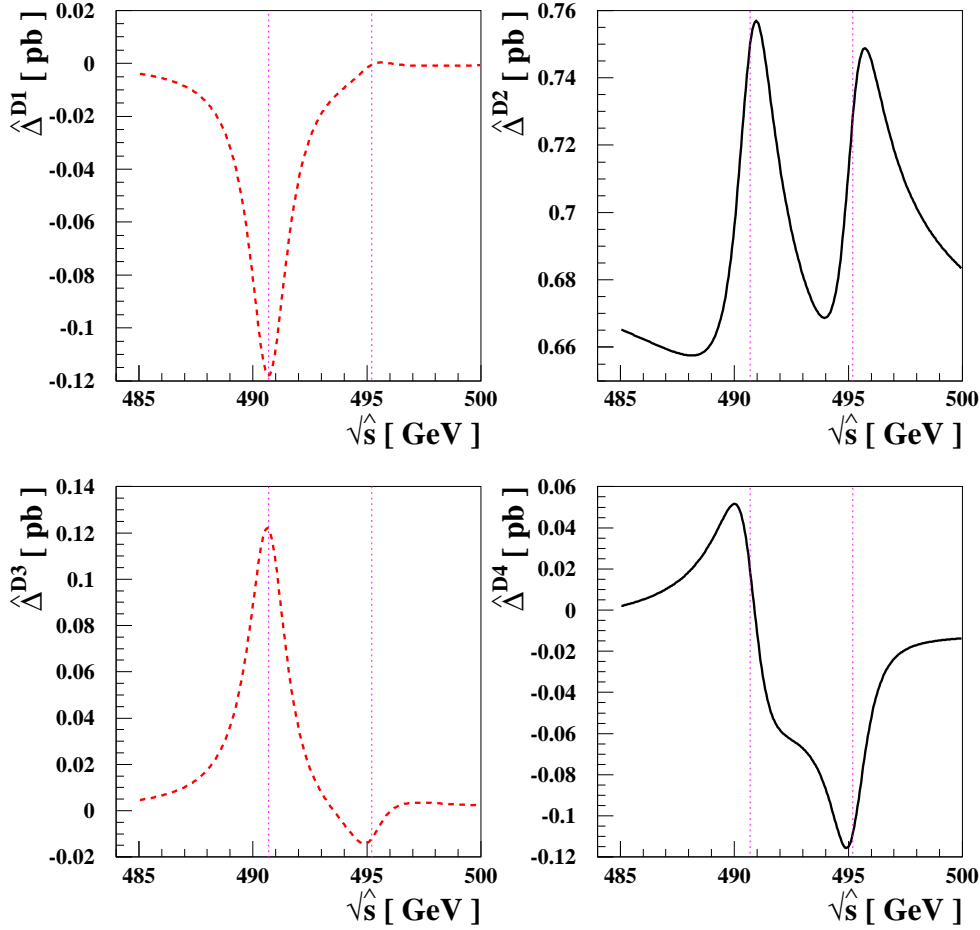


**Figure 18:** The cross sections  $\hat{\Delta}^{D_i}(\gamma(\lambda)\gamma(\lambda) \rightarrow t(\sigma)\bar{t}(\bar{\sigma}))$  (Case III) for the parameter set (4.1) as functions of  $\sqrt{\hat{s}}$ .

## References

- [1] For reviews, see, H.P. Nilles, Phys. Rep. **110** (1984) 1; H. Haber and G. Kane, Phys. Rep. **117** (1985) 75; J.F. Gunion, H.E. Haber, G.L. Kane and S. Dawson, *The Higgs Hunter's Guide*, (Addison-Wesley, Reading, MA, 1990).
- [2] S. Y. Choi, J. Kalinowski, G. Moortgat-Pick and P. M. Zerwas, Eur. Phys. J. C **22** (2001) 563; S. Y. Choi, A. Djouadi, M. Guchait, J. Kalinowski, H. S. Song and P. M. Zerwas, Eur. Phys. J. C **14** (2000) 535; A. Bartl, H. Fraas, O. Kittel and W. Majerotto, Phys. Rev. D **69** (2004) 035007; S. Y. Choi, M. Drees and B. Gaissmaier, Phys. Rev. D **70** (2004) 014010.
- [3] A. Bartl, S. Hesselbach, K. Hidaka, T. Kernreiter and W. Porod, Phys. Lett. B **573** (2003) 153; Phys. Rev. D **70** (2004) 035003; S. Y. Choi, Phys. Rev. D **69** (2004) 096003; S. Y. Choi, M. Drees, B. Gaissmaier and J. Song, Phys. Rev. D **69** (2004)

- 035008; S. Y. Choi and Y. G. Kim, Phys. Rev. D **69** (2004) 015011; J. A. Aguilar-Saavedra, Phys. Lett. B **596** (2004) 247; Nucl. Phys. B **697** (2004) 207; T. Gajdosik, R. M. Godbole and S. Kraml, JHEP **0409** (2004) 051.
- [4] For an extensive review, see D. J. H. Chung, L. L. Everett, G. L. Kane, S. F. King, J. Lykken and L. T. Wang, hep-ph/0312378.
- [5] A. Pilaftsis, Phys. Rev. D **58** (1998) 096010; Phys. Lett. B **435** (1998) 88.
- [6] J. Ellis, S. Ferrara and D.V. Nanopoulos, Phys. Lett. B **114** (1982) 231; W. Buchmüller and D. Wyler, Phys. Lett. B **121** (1983) 321; J. Polchinski and M. Wise, Phys. Lett. B **125** (1983) 393; F. del Aguila, M. Gavela, J. Grifols and A. Mendez, Phys. Lett. B **126** (1983) 71; M. Dugan, B. Grinstein and L. Hall, Nucl. Phys. B **255** (1985) 413; R. Garisto and J.D. Wells, Phys. Rev. D **55** (1997) 1611.
- [7] T. Ibrahim and P. Nath, Phys. Rev. D **58** (1998) 111301; Phys. Rev. D **61** (2000) 093004; M. Brhlik, L. Everett, G.L. Kane and J. Lykken, Phys. Rev. Lett. **83** (1999) 2124; Phys. Rev. D **62** (2000) 035005; S. Pokorski, J. Rosiek and C.A. Savoy, Nucl. Phys. B **570** (2000) 81; E. Accomando, R. Arnowitt and B. Dutta, Phys. Rev. D **61** (2000) 115003; A. Bartl, T. Gajdosik, W. Porod, P. Stockinger and H. Stremnitzer, Phys. Rev. D **60** (1999) 073003; T. Falk, K.A. Olive, M. Pospelov and R. Roiban, Nucl. Phys. B **560** (1999) 3; S.A. Abel, S. Khalil and O. Lebedev, Nucl. Phys. B **606** (2001) 151.
- [8] For two-loop Higgs-mediated contributions to EDMs in the CP-violating MSSM, see D. Chang, W.-Y. Keung and A. Pilaftsis, Phys. Rev. Lett. **82** (1999) 900; A. Pilaftsis, Nucl. Phys. B **644** (2002) 263; D. A. Demir, O. Lebedev, K. A. Olive, M. Pospelov and A. Ritz, Nucl. Phys. B **680** (2004) 339.
- [9] For recent studies, see P.H. Chankowski and L. Slawianowska, Phys. Rev. D **63** (2001) 054012; C.S. Huang, W. Liao, Q.-S. Yuan and S.-H. Zhu, Phys. Rev. D **63** (2001) 114021; D. A. Demir and K. A. Olive, Phys. Rev. D **65** (2002) 034007; M. Boz and N. K. Pak, Phys. Lett. B **531** (2002) 119; A. J. Buras, P. H. Chankowski, J. Rosiek and L. Slawianowska, Nucl. Phys. B **659** (2003) 3; T. Ibrahim and P. Nath, Phys. Rev. D **67** (2003) 016005; Phys. Rev. D **67** (2003) 095003.
- [10] For the general resummed form of the effective Lagrangian for Higgs-mediated FCNC interactions, see, A. Dedes and A. Pilaftsis, Phys. Rev. D **67** (2003) 015012.
- [11] A. Pilaftsis and C.E.M. Wagner, Nucl. Phys. B **553** (1999) 3.

- [12] D.A. Demir, Phys. Rev. D **60** (1999) 055006.
- [13] S.Y. Choi, M. Drees and J.S. Lee, Phys. Lett. B **481** (2000) 57.
- [14] M. Carena, J. Ellis, A. Pilaftsis and C.E.M. Wagner, Nucl. Phys. B **586** (2000) 92.
- [15] T. Ibrahim and P. Nath, Phys. Rev. D **63** (2001) 035009; Phys. Rev. D **66** (2002) 015005; T. Ibrahim, Phys. Rev. D **64** (2001) 035009; S. W. Ham, S. K. Oh, E. J. Yoo, C. M. Kim and D. Son, Phys. Rev. D **68** (2003) 055003; T. Ibrahim, P. Nath and A. Psinas, Phys. Rev. D **70** (2004) 035006.
- [16] M. Carena, J. Ellis, A. Pilaftsis and C.E.M. Wagner, Nucl. Phys. B **625** (2002) 345.
- [17] G.L. Kane and L.-T. Wang, Phys. Lett. B **488** (2000) 383.
- [18] S. Heinemeyer, Eur. Phys. J. C **22** (2001) 521.
- [19] E. Akhmetzyanova, M. Dolgoplov and M. Dubinin, hep-ph/0405264; I. F. Ginzburg and M. Krawczyk, hep-ph/0408011.
- [20] A. Pilaftsis, Nucl. Phys. B **504** (1997) 61.
- [21] J. R. Ellis, J. S. Lee and A. Pilaftsis, Phys. Rev. D **70** (2004) 075010; J.S. Lee, hep-ph/0409020.
- [22] M. Carena, J. Ellis, A. Pilaftsis and C.E.M. Wagner, Phys. Lett. B **495** (2000) 155.
- [23] S.Y. Choi and J.S. Lee, Phys. Rev. D **61** (2000) 015003; S.Y. Choi, K. Hagiwara and J.S. Lee, Phys. Rev. D **64** (2001) 032004; S. Y. Choi, M. Drees, J. S. Lee and J. Song, Eur. Phys. J. C **25** (2002) 307.
- [24] M. Carena, J. Ellis, S. Mrenna, A. Pilaftsis and C.E.M. Wagner, Nucl. Phys. B **659** (2003) 145.
- [25] W. Bernreuther and A. Brandenburg, Phys. Lett. B **314** (1993) 104; W. Bernreuther and A. Brandenburg, Phys. Rev. D **49** (1994) 4481; A. Dedes and S. Moretti, Phys. Rev. Lett. **84** (2000) 22; Nucl. Phys. B **576** (2000) 29; S.Y. Choi and J.S. Lee, Phys. Rev. D **61** (2000) 115002; S.Y. Choi, K. Hagiwara and J.S. Lee, Phys. Lett. B **529** (2002) 212; A. Arhrib, D. K. Ghosh and O.C. Kong, Phys. Lett. B **537** (2002) 217; E. Christova, H. Eberl, W. Majerotto and S. Kraml, Nucl. Phys. B **639** (2002) 263; JHEP **0212** (2002) 021; W. Khater and P. Osland, Nucl. Phys. B **661** (2003) 209; F. Borzumati, J. S. Lee and W. Y. Song, Phys. Lett. B **595** (2004) 347.

- [26] B.E. Cox, J.R. Forshaw, J.S. Lee, J.W. Monk and A. Pilaftsis, Phys. Rev. D **68** (2003) 075004; A.G. Akeroyd, Phys. Rev. D **68** (2003) 077701.
- [27] V.A. Khoze, A.D. Martin and M.G. Ryskin, hep-ph/0401078.
- [28] B. Grzadkowski, J. F. Gunion and J. Kalinowski, Phys. Rev. D **60** (1999) 075011; A.G. Akeroyd and A. Arhrib, Phys. Rev. D **64** (2001) 095018.
- [29] D. Atwood and A. Soni, Phys. Rev. D **52** (1995) 6271; B. Grzadkowski and J.F. Gunion, Phys. Lett. B **350** (1995) 218; A. Pilaftsis, Phys. Rev. Lett. **77** (1996) 4996; S.Y. Choi and J.S. Lee, Phys. Rev. D **61** (2000) 111702; E. Asakawa, S.Y. Choi and J.S. Lee, Phys. Rev. D **63** (2001) 015012; S.Y. Choi, M. Drees, B. Gaissmaier and J.S. Lee, Phys. Rev. D **64** (2001) 095009; M.S. Berger, Phys. Rev. Lett. **87** (2001) 131801; C. Blochinger *et al.*, hep-ph/0202199.
- [30] S. Y. Choi and J. S. Lee, Phys. Rev. D **62** (2000) 036005; J. S. Lee, hep-ph/0106327; S. Y. Choi, B. C. Chung, P. Ko and J. S. Lee, Phys. Rev. D **66** (2002) 016009; S. Y. Choi, J. Kalinowski, J. S. Lee, M. M. Muhlleitner, M. Spira and P. M. Zerwas, hep-ph/0404119.
- [31] E. Asakawa, S. Y. Choi, K. Hagiwara and J.S. Lee, Phys. Rev. D **62** (2000) 115005; R. M. Godbole, S. D. Rindani and R. K. Singh, Phys. Rev. D **67** (2003) 095009; E. Asakawa and K. Hagiwara, Eur. Phys. J. C **31** (2003) 351.
- [32] R. M. Godbole, S. Kraml and R. K. Singh, arXiv:hep-ph/0409199.
- [33] S. Y. Choi, J. Kalinowski, Y. Liao and P. M. Zerwas, hep-ph/0407347.
- [34] J.M. Cornwall, Phys. Rev. D **26** (1982) 1453; J. M. Cornwall and J. Papavassiliou, Phys. Rev. D **40** (1989) 3474; J. Papavassiliou, Phys. Rev. D **41** (1990) 3179; Phys. Rev. D **50** (1994) 5958; G. Degrassi and A. Sirlin, Phys. Rev. D **46** (1992) 3104. S. Hashimoto, J. Kodaira, Y. Yasui, and K. Sasaki, Phys. Rev. D **50** (1994) 7066; N.J. Watson, Phys. Lett. B **349** (1995) 155; D. Binosi, J. Phys. G **30** (2004) 1021.
- [35] J. Papavassiliou and A. Pilaftsis, Phys. Rev. Lett. **80** (1998) 2785; Phys. Rev. D **58** (1998) 053002.
- [36] J. S. Lee, A. Pilaftsis, M. Carena, S. Y. Choi, M. Drees, J. R. Ellis and C. E. M. Wagner, Comput. Phys. Commun. **156** (2004) 283 [arXiv:hep-ph/0307377].
- [37] K. Hagiwara and D. Zeppenfeld, Nucl. Phys. B **274** (1986) 1.

- [38] I. F. Ginzburg, G. L. Kotkin, S. L. Panfil, V. G. Serbo and V. I. Telnov, Nucl. Instrum. Meth. **A219** (1984) 5; B. Badelek *et al.* [ECFA/DESY Photon Collider Working Group Collaboration], arXiv:hep-ex/0108012.
- [39] D. Asner *et al.*, Eur. Phys. J. C **28** (2003) 27 [arXiv:hep-ex/0111056].
- [40] E. Asakawa, J. i. Kamoshita, A. Sugamoto and I. Watanabe, Eur. Phys. J. C **14** (2000) 335.
- [41] For recent studies, see, M. Carena, M. Quirós and C.E.M. Wagner, Nucl. Phys. **B524** (1998) 3; M. Laine and K. Rummukainen, Nucl. Phys. **B535** (1998) 423; K. Funakubo, Prog. Theor. Phys. **102** (1999) 389; J. Grant and M. Hindmarsh, Phys. Rev. **D59** (1999) 116014; M. Losada, Nucl. Phys. **B569** (2000) 125; J. M. Cline, M. Joyce and K. Kainulainen, JHEP **0007** (2000) 018; M. Carena, J.M. Moreno, M. Quiros, M. Seco and C.E.M. Wagner, Nucl. Phys. **B599** (2001) 158; M. Laine and K. Rummukainen, Nucl. Phys. **B597** (2001) 23; K. Kainulainen, T. Prokopec, M. G. Schmidt and S. Weinstock, JHEP **0106** (2001) 031.

**Table 1:** All polarization-dependent cross sections considered in units of  $\frac{\beta_f N_C}{32\pi} \left(\frac{\alpha m_f}{4\pi v^2}\right)^2$ . The CP and CPT parities of the cross sections are also shown in the first column. Equivalent quantities are given in the last column.

Cross sections [CP, CPT]	Expressions	Equivalents
$\hat{\sigma}[+, +]$	$(\mathcal{Y}_{++} + \mathcal{Y}_{+-} + \mathcal{Y}_{-+} + \mathcal{Y}_{--})/4$	$\hat{\Sigma}^{D_1}$
$\hat{\Delta}_1[-, -]$	$\mathcal{Y}_{++} - \mathcal{Y}_{--}$	
$\hat{\Delta}_2[-, -]$	$\mathcal{Y}_{+-} - \mathcal{Y}_{-+}$	
$\hat{\Sigma}^{A_1}[+, +]$	$[(\mathcal{Y}_{++} + \mathcal{Y}_{+-} + 2\mathcal{W}_+) + (\mathcal{Y}_{-+} + \mathcal{Y}_{--} + 2\mathcal{W}_-)]/4$	
$\hat{\Sigma}^{A_2}[+, +]$	$[\mathcal{W}_+ + \mathcal{W}_-]/2$	$\hat{\Sigma}^{A_1} - \hat{\Sigma}^{A_2} = \hat{\sigma}$
$\hat{\Sigma}^{B_1}[-, -]$	$[(\mathcal{Y}_{++} - \mathcal{Y}_{+-}) + (\mathcal{Y}_{-+} - \mathcal{Y}_{--})]/4$	$(\hat{\Delta}_1 - \hat{\Delta}_2)/4, \hat{\Delta}^{D_1}$
$\hat{\Sigma}^{B_2}[-, +]$	$\Im[\mathcal{X}_+ + \mathcal{X}_-]/2$	
$\hat{\Sigma}^{B_3}[+, +]$	$\Re[\mathcal{X}_+ + \mathcal{X}_-]/2$	
$\hat{\Sigma}^{C_1}[-, +]$	$-\Im[(\mathcal{Z}_{++} - \mathcal{Z}_{+-}) + (\mathcal{Z}_{-+} - \mathcal{Z}_{--})]/2$	
$\hat{\Sigma}^{C_2}[+, +]$	$-\Re[(\mathcal{Z}_{++} + \mathcal{Z}_{+-}) + (\mathcal{Z}_{-+} + \mathcal{Z}_{--})]/2$	
$\hat{\Sigma}^{C_3}[+, -]$	$-\Im[(\mathcal{Z}_{++} + \mathcal{Z}_{+-}) + (\mathcal{Z}_{-+} + \mathcal{Z}_{--})]/2$	
$\hat{\Sigma}^{C_4}[-, -]$	$-\Re[(\mathcal{Z}_{++} - \mathcal{Z}_{+-}) + (\mathcal{Z}_{-+} - \mathcal{Z}_{--})]/2$	
$\hat{\Delta}^{A_1}[-, -]$	$[(\mathcal{Y}_{++} + \mathcal{Y}_{+-} + 2\mathcal{W}_+) - (\mathcal{Y}_{-+} + \mathcal{Y}_{--} + 2\mathcal{W}_-)]/4$	$(\hat{\Delta}_1 + \hat{\Delta}_2)/4, \hat{\Sigma}^{D_2}$
$\hat{\Delta}^{A_2}[-, -]$	$[\mathcal{W}_+ - \mathcal{W}_-]/2$	0
$\hat{\Delta}^{B_1}[+, +]$	$[(\mathcal{Y}_{++} - \mathcal{Y}_{+-}) - (\mathcal{Y}_{-+} - \mathcal{Y}_{--})]/4$	$\hat{\Delta}^{D_2}$
$\hat{\Delta}^{B_2}[+, -]$	$\Im[\mathcal{X}_+ - \mathcal{X}_-]/2$	
$\hat{\Delta}^{B_3}[-, -]$	$\Re[\mathcal{X}_+ - \mathcal{X}_-]/2$	
$\hat{\Delta}^{C_1}[+, -]$	$-\Im[(\mathcal{Z}_{++} - \mathcal{Z}_{+-}) - (\mathcal{Z}_{-+} - \mathcal{Z}_{--})]/2$	
$\hat{\Delta}^{C_2}[-, -]$	$-\Re[(\mathcal{Z}_{++} + \mathcal{Z}_{+-}) - (\mathcal{Z}_{-+} + \mathcal{Z}_{--})]/2$	
$\hat{\Delta}^{C_3}[-, +]$	$-\Im[(\mathcal{Z}_{++} + \mathcal{Z}_{+-}) - (\mathcal{Z}_{-+} + \mathcal{Z}_{--})]/2$	
$\hat{\Delta}^{C_4}[+, +]$	$-\Re[(\mathcal{Z}_{++} - \mathcal{Z}_{+-}) - (\mathcal{Z}_{-+} - \mathcal{Z}_{--})]/2$	
$\hat{\Sigma}^{D_1}[+, +]$	$[(\mathcal{Y}_{++} + \mathcal{Y}_{-+}) + (\mathcal{Y}_{+-} + \mathcal{Y}_{--})]/4$	$\hat{\sigma}$
$\hat{\Sigma}^{D_2}[-, -]$	$[(\mathcal{Y}_{++} - \mathcal{Y}_{-+}) + (\mathcal{Y}_{+-} - \mathcal{Y}_{--})]/4$	$(\hat{\Delta}_1 + \hat{\Delta}_2)/4, \hat{\Delta}^{A_1}$
$\hat{\Sigma}^{D_3}[+, +]$	$-\Re[\tilde{\mathcal{X}}_+ + \tilde{\mathcal{X}}_-]/2$	
$\hat{\Sigma}^{D_4}[-, +]$	$\Im[\tilde{\mathcal{X}}_+ + \tilde{\mathcal{X}}_-]/2$	
$\hat{\Delta}^{D_1}[-, -]$	$[(\mathcal{Y}_{++} + \mathcal{Y}_{-+}) - (\mathcal{Y}_{+-} + \mathcal{Y}_{--})]/4$	$(\hat{\Delta}_1 - \hat{\Delta}_2)/4, \hat{\Sigma}^{B_1}$
$\hat{\Delta}^{D_2}[+, +]$	$[(\mathcal{Y}_{++} - \mathcal{Y}_{-+}) - (\mathcal{Y}_{+-} - \mathcal{Y}_{--})]/4$	$\hat{\Delta}^{B_1}$
$\hat{\Delta}^{D_3}[-, -]$	$-\Re[\tilde{\mathcal{X}}_+ - \tilde{\mathcal{X}}_-]/2$	
$\hat{\Delta}^{D_4}[+, -]$	$\Im[\tilde{\mathcal{X}}_+ - \tilde{\mathcal{X}}_-]/2$	